AFRL-SR-AR-TR-04-

0646

REPORT DOCUMENTATION PAGE

1. AGENCY USE ONLY *(Leave blank)*	2. REPORT DATE	3. REPORT TYPE AND DATES COVERED
		15 May 2000 - 14 May 2004 FINAL

4. TITLE AND SUBTITLE
(DEPSCOR FY00) A Novel Processing Technique for Growing Bulk Gallium Nitride Ingots form Gallium Melt

5. FUNDING NUMBERS
61103D
3484/BS

6. AUTHOR(S)
Professor Sunkara

7. PERFORMING ORGANIZATION NAME(S) AND ADDRESS(ES)
UNIVERSITY OF LOUISVILLE RESEARCH FOUNDATION
CONTROLLER'S OFFICE - SERVICE COMPLEX
2301 S 3RD STREET
LOUISVILLE KY 40292-0001

8. PERFORMING ORGANIZATION REPORT NUMBER

9. SPONSORING/MONITORING AGENCY NAME(S) AND ADDRESS(ES)
AFOSR/NE
4015 WILSON BLVD
SUITE 713
ARLINGTON VA 22203

10. SPONSORING/MONITORING AGENCY REPORT NUMBER
F49620-00-1-0310

11. SUPPLEMENTARY NOTES

12a. DISTRIBUTION AVAILABILITY STATEMENT
DISTRIBUTION STATEMENT A: Unlimited

12b. DISTRIBUTION CODE

13. ABSTRACT *(Maximum 200 words)*

In summary, a new process is being developed to obtain free standing, large area, 'near~ ~ single crystal quality GuN flakes (highly oriented GaN films) promising as native substrates for homoepitaxial growth of device quality, low-defect density GaN layers. However, the experiments to date resulted only in GaN flakes of sizes around 1 cm2 due to the following reasons: (a) the wetting and flow of molten Ga affected the flatness of the Ga film surfaces during the nucleation and coalescence of GaN crystals (b) the flow of Ga through cracks or discontinuities within the films limited the area of highly oriented GaN films- Currently, two types of experiments involving substrate stage rotation and in-situ Ga delivery are being conducted to overcome the above difficulties. Similarly, MOCVD deposition studies onto GaN flakes are planned for making several mm thick ingots.

14. SUBJECT TERMS

15. NUMBER OF PAGES

16. PRICE CODE

17. SECURITY CLASSIFICATION OF REPORT	18. SECURITY CLASSIFICATION OF THIS PAGE	19. SECURITY CLASSIFICATION OF ABSTRACT	20. LIMITATION OF ABSTRACT
Unclassified	Unclassified	Unclassified	UL

A Novel Processing Technique for Growing Bulk Gallium Nitride Ingots from Gallium Melt

DEPSCoR Project: AFOSR (F49620-00-1-0310)
05/15/2000--------04/30/2004

Final Report

Submitted by:

P.I.: Mahendra K. Sunkara, Associate Professor of Chemical Engineering

Research Assistants:
Hongwei Li, Hari Chandrasekaran, Sreeram Vaddiraju

Advanced Materials Synthesis & Characterization Laboratory,
Department of Chemical Engineering, University o Louisville,
Louisville, KY, 40292
Phone: 502-852-0500
Fax: 502-852-6355
http://www.cvd.louisville.edu/

Submitted to:

Dr. Gerald L. Witt
Program Manager, AFOSR/NE 4015
Wilson Blvd, Room 713 Arlington, VA 22203-1954
Gerald.witt@afosr.af.mil

Final Report Dec. 2004

TABLE OF CONTENTS

EXECUTIVE SUMMARY

In this work, we proposed and demonstrated an innovative concept of self-oriented GaN crystal growth to produce single crystal quality films over large areas. In this concept, the GaN crystals nucleate from nitrogen saturated gallium melts at sub-atmospheric pressures and coalesce over molten gallium surfaces in a self-oriented fashion. The main objectives of this project were: (a) demonstrate the concept, i.e., highly oriented films with low-angle grain boundaries without the help of hetero-epitaxial, single crystal substrates; (b) produce "near" single crystal quality films over areas exceeding 1 cm^2 and characterize the films for dislocations within grains and at grain boundaries; and (c) determine whether one can thicken the films using in-situ Ga delivery and growth via liquid phase epitaxy (LPE) for making several mm thick ingots.

First, a set of experiments was performed to understand the bulk nucleation and growth process of GaN from molten Ga, the morphologies of GaN crystals and various nitridation conditions in our ECR plasma reactor. Second, another set of nitridation experiments were performed using thick Ga film covered amorphous substrates to obtain large area flakes. Extensive characterization using X-ray Diffraction (XRD) and transmission electron microscopy (TEM) was then performed to understand the orientation of the resulting GaN films over large areas (> 5 mm-sized flakes) and to understand the structure of boundaries between adjacent crystals. Finally, preliminary experiments employing substrate stage rotation during nitridation were performed to see whether rotation helps in increasing the area of the resulting self-oriented GaN film.

The results from the controlled nucleation experiments showed that the sizes of GaN nuclei increase with the initial gallium volume or thickness used and the density decreases with thickness confirming that the nucleation in this case is a bulk phenomenon. Self oriented GaN flakes larger than 10 mm in size were obtained with individual domain sizes as large as a few microns. The thickness of the self-oriented GaN flakes was increased from 2 microns to 20 microns with increased nitridation time scales. The TEM analysis of the self-oriented, free-standing GaN flakes did not indicate any dislocation crops within the GaN crystals but showed the presence of stacking faults in the c-plane growth direction. High-resolution TEM (HRTEM) analysis indicated low-angle grain boundaries and no apparent dislocation crops. The attachments between adjacent crystals varied from perfect to twisted (less than 10 degrees). Raman and PL optical characterization indicated variations in yellow luminescence intensity between samples grown at different conditions but no generalizations were obtained. UV Photoelectron Spectroscopy (UPS) and Scanning Tunneling Spectroscopy (STS) studies on the GaN samples allowed us to determine the band gap of the bulk grown GaN films to be about 3.4 eV.

A set of studies was focused on understanding the mechanistic aspects of the self-oriented growth during initial and subsequent thickening with increased nitridation timescales. Based on these studies, the self-oriented growth to form thick single crystal quality films is hypothesized to take place with the following sequence of events: (a) nitrogen dissolution into molten Ga from the activated nitrogen gas phase; (b) nucleation

of GaN crystals; (c) flow of the nitrogenated Ga melt aligns the platelet shaped crystals with their c-planes parallel to the Ga surface; (d) the coalescence of crystals on Ga occurs through self-orientation upon physical impingement with each other on molten Ga due to rotational mobility; and (e) subsequent growth (thickening) of the self-oriented GaN film occurs through liquid phase epitaxy (LPE).

In summary, a new process is being developed to obtain free standing, large area, "near" single crystal quality GaN flakes (highly oriented GaN films) promising as native substrates for homoepitaxial growth of device quality, low-defect density GaN layers. However, the experiments to date resulted only in GaN flakes of sizes around 1 cm^2 due to the following reasons: (a) the wetting and flow of molten Ga affected the flatness of the Ga film surfaces during the nucleation and coalescence of GaN crystals (b) the flow of Ga through cracks or discontinuities within the films limited the area of highly oriented GaN films. Currently, two types of experiments involving substrate stage rotation and in-situ Ga delivery are being conducted to overcome the above difficulties. Similarly, MOCVD deposition studies onto GaN flakes are planned for making several mm thick ingots.

ACCOMPLISHMENTS

Technical Results:

- Self-orientated growth of GaN films on top of gallium. Cross-sectional TEM micrographs showed that the resulting GaN films are free from dislocation crops inside the grains, and HRTEM micrographs of the grain boundaries showed sharp interfaces with both twisted and perfect attachments
- Self-oriented GaN flakes as large as 1 cm^2 in area and thicknesses as high as 19 microns were obtained through the nitridation of Ga film covered amorphous quartz substrates.
- Assembled a rotating stage (2 inch) that can operate at speeds > 2000 rpm and reach temperatures > 900 C for our electron cyclotron resonance (ECR) reactor. Preliminary experiments were conducted. A systematic set of nitridation experiments are currently being conducted for understanding the effect of rotation on self-oriented growth.
- Experiments were conducted for determining the nucleation and growth kinetics of GaN as a function of the original Ga thickness. Based on the results, it was concluded that the nucleation of GaN during the nitridation of Ga films with thicknesses less than a few mm is a bulk phenomenon rather than a surface phenomenon.
- GaN growth using very thin gallium films resulted in nanocrystalline GaN films on 2.0-inch amorphous quartz substrates.
- Bulk GaN using thin gallium films on single crystal sapphire substrates resulted in epitaxial growth of single crystal GaN films with the underlying substrate at certain regions, which was confirmed with synchrotron topography characterization. The scintillation behavior of GaN films grown on sapphire substrates indicated sub-nanosecond decay times for Cathodoluminescence (CL).
- Scanning Tunneling Spectroscopy (STS) of GaN films showed a bandgap between 3.3-3.4 eV and Ultraviolet Photoelectron Spectroscopy (UPS) indicated n-type conductivity.
- One dimensional tubes, straight nanowires (~10 nm diameter and hundreds of microns long), faceted tapered nanowires and star-shaped morphologies were obtained when hydrogen was added to the gas phase. Conclusive evidence was obtained demonstrating the multiple nucleation and growth of nanowires directly from Ga melts with the addition of hydrogen to nitrogen plasmas during nitridation. Synthesized InN nanowire arrays onto HOPG (graphite) and Sapphire, integrated them into devices, and measured the bandgap to be around 0.8 eV.
- Homo-epitaxial growth on GaN nanowires (sub-20 nm diameter and hundreds of microns long) allowed us to conclude that the surface transport of adatoms on nanowires could be ballistic and will pave the way for more experiments leading to nano-heterostructures that can be easily integrated into devices.

Outcomes:

- Three Ph.D. level students in chemical engineering are expected to graduate in 2005. One M.S. thesis was completed in 2002.
- Two directly related patent applications on the process have been filed. One of the applications has already been approved. Two other related patents on nanowire synthesis have been approved.
- Six (6) publications resulted directly from the bulk synthesis of GaN with several more submissions planned in the near future.
- This DEPSCoR project on bulk nucleation from molten Ga resulted in another research finding, i.e., using low-melting metal melts for mediating the bulk nucleation and growth of nanowires of several inorganic materials. This effort resulted in an additional ten (10) publications, over 15 invited talks and four patent applications (one issued, one allowed and others pending).
- Using the results partially from this project, the PI was able to attract funding from NSF and the State of KY to establish a UHV facility for surface science experiments (XPS, UPS, AES, STM).
- Subsequent funding (about $100K) for two years has been secured from the Kentucky Science & Engineering Foundation (KSEF) for fundamental studies on the nucleation and growth of GaN from molten Ga using atomic nitrogen.
- A follow-on proposal is being submitted through the DEPSCoR program.

PROJECT REPORT

I. Introduction and Background

Group III-nitrides are direct, wide band gap semiconductor materials that have applications in blue light emitting diodes (LED) [1], blue laser diodes (LD) [2], and high temperature/high power field effect transistors (FET) [3]. Their ability to form continuous alloys allows for a wide range of band gaps from 0.7eV (InN) to 6.2eV (AlN), which is essential for producing specific wavelength emitters. Therefore, there has been a tremendous effort to grow large area, low defect density single crystal GaN. However, due to the unavailability of lattice matched substrates, hetero-epitaxy on substrates such as sapphire or SiC is currently employed using metal organic chemical vapor deposition (MOCVD)[4], molecular beam epitaxy (MBE)[5] or hydride vapor phase epitaxy (HVPE)[6] techniques. Lattice mismatch and differences in the thermal expansion properties between GaN and the substrates employed cause a high density of dislocations on the order of 10^9-$10^{10}/cm^2$ and stresses in the resulting films [7-8]. Engineered techniques such as lateral epitaxial overgrowth (LEO) [9] or pendeo-epitaxy [10] have achieved significant reductions in the dislocation density down to 10^6 to $10^7/cm^2$. However, homoepitaxy on high quality GaN substrates with dislocation densities less than $10^4/cm^2$ is preferred [11].

Despite the huge technological interest, the progress in high power blue lasers and long-term applications has been slow due to the unavailability of low defect density GaN wafers. GaN crystals cannot be grown using typical Bridgman or Czochralski type techniques due to the fact that decomposition occurs prior to melting. The best way to obtain GaN crystals with low defect densities is to use bulk synthesis. The maximum size of GaN crystals from bulk growth under high temperature, high-pressure (>1500 °C, >15kbar) conditions is 17 mm with dislocation densities lower than $10^3/cm^2$ [12], but further scale-up is complicated due to the extreme conditions involved. Other techniques such as physical vapor transport (PVT) [13], ammonothermal [14] and sodium flux solution growth [15] also show promise, but the crystal size is limited to the mm scale. The inherent difficulties with bulk synthesis require further understanding. In 1997, Angus, et al., demonstrated the bulk growth of GaN at low pressures using atomic nitrogen from the gas phase [16]. These experiments resulted in a polycrystalline mass due to spontaneous nucleation and uncontrolled growth [16]. As illustrated below, thermodynamics suggest that the use of atomic nitrogen allows for GaN formation even at sub-atmospheric pressures.

$Ga(l) + 1/2N_2(g) \rightarrow GaN(s)$ (p_{equ} = 1500 bar @ 1500K using molecular nitrogen)
$Ga(l) + N(g) \rightarrow GaN(s)$ ($p_{equ} = 10^{-11}$ bar @ 1500K using atomic nitrogen)

The growth of GaN using ammonia as the nitrogen source can take place through two different reaction mechanisms. One is the direct dissolution of ammonia into gallium and the precipitation of GaN:

$Ga(l) + NH_3(g) \rightarrow GaN + 3/2\ H_2$ ($p_{equ} \sim 1$ bar @ 1500K using ammonia)

The other mechanism involves the dissociation of ammonia into active nitrogen species, which then dissolves into gallium:

$NH_3(g) \rightarrow N(g) + 3/2\ H_2(g)$ (dissociation of ammonia)
$Ga(l) + N(g) \rightarrow GaN(s)$ (dissolution of atomic nitrogen)

Ammonia dissociates into atomic nitrogen and hydrogen on heated surfaces. In this manner, the ammonothermal approach and low-pressure bulk synthesis approach using atomic hydrogen are similar except for the operating pressures. However, as shown later, the presence of atomic/molecular hydrogen could affect the morphology of the resulting GaN crystals.

Using low-pressure bulk synthesis, we proposed a concept for the self-oriented growth of GaN over large areas on amorphous substrates, shown in Fig. 1. In this concept, we hypothesized that the orientation of GaN crystals could be influenced by the applied flow (using rotation), and the self-assembly of these platelet shaped crystals is expected during coalescence to produce a highly oriented film with low-angle grain boundaries. The high mobility of the crystals on liquid Ga permits the self-orientation. So, our main goal was to study whether one can achieve self-oriented growth over large areas (> cm^2) without the help of hetero-epitaxy with underlying single crystal substrate templates. The other objectives were to understand the nucleation and growth of GaN from Ga melts with activated nitrogen dissolution.

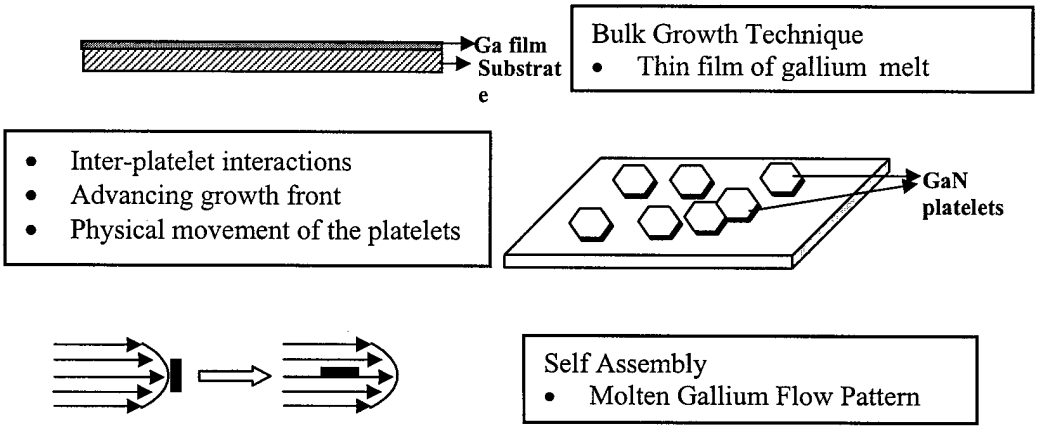

Figure 1. Self-Assembly of bulk grown GaN on molten gallium. The flow can be self-induced by the wetting and spreading of nitrogenated gallium melts. Applied forces from rotation of the substrate stage also cause flow fields that enhance the orientation of the GaN platelets during the early stages of growth.

II. Experiments and Results

All nitridation experiments excluding the InN nanowire experiments discussed later, were performed in a water-cooled double wall vacuum chamber with an ASTeX®

Model AX4500 ECR plasma source, shown in Fig. 2. Prior to nitridation experiments, H_2 plasma at room temperature was used for about 30 minutes to remove any possible native oxide on the surface of the gallium.

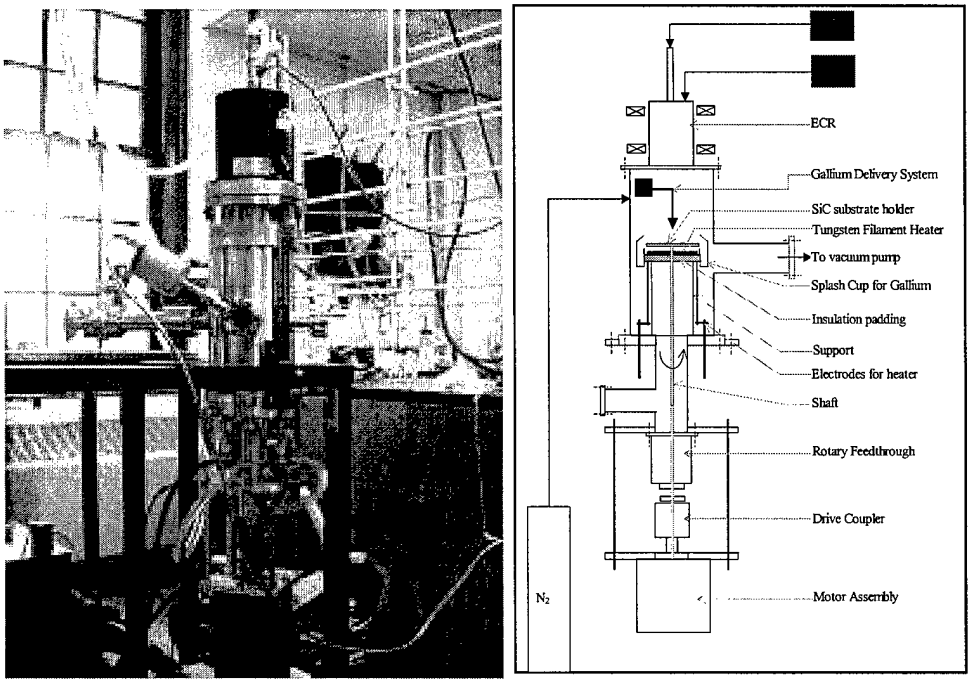

Figure 2. ECR-MW reactor with rotating heated substrate stage assembly. The base flange can be interchanged to fit in a flat Boralectric® heater substrate stage assembly or RF biased substrate stage.

1.0 Bulk pool experiments

Subsequently, the gallium was exposed to N_2 plasma and heated to 900-1000°C for 1-7 hours at a chamber pressure of 100 mTorr.

The first sets of experiments were performed using bulk pools of molten gallium without any substrate. In these experiments, we observed that the GaN crystals formed a crust in the shape of a hollow dome over the molten gallium. The c-plane of the GaN crust was found to be parallel to the surface of the dome. Thus the GaN film, although c-plane oriented, was not flat, as shown in the schematic in Fig.3.

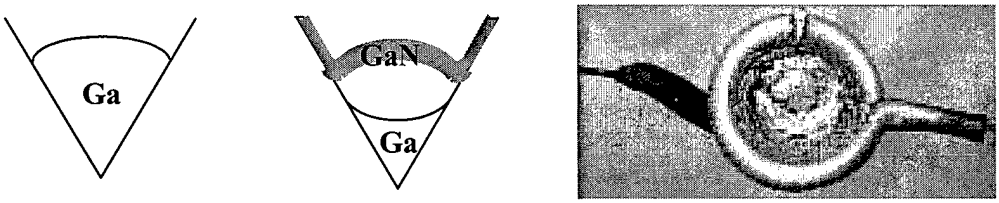

(a) (b) (c)

Figure 3. (a) The shape of the molten gallium before nitridation; (b) gallium spreads during nitridation forming a hollow dome shaped GaN crust; (c) picture of the crucible after nitridation clearly shows that the gallium spread from underneath along the walls of the crucible all the way to the top.

In order to get a flat oriented GaN film, experiments were performed with p-BN or amorphous quartz substrates immersed and placed above bulk pools of gallium (Fig. 4). The experiments yielded self-oriented GaN flakes several mm in size [Fig. 5(a) & (b)]. These flakes contain self-aligned monolayers of GaN crystals as shown in Fig. 5 (c) & (d). XRD and Raman spectra in Figs. 5(e) & (f) show strong c-plane texturing and good quality hexagonal GaN, respectively.

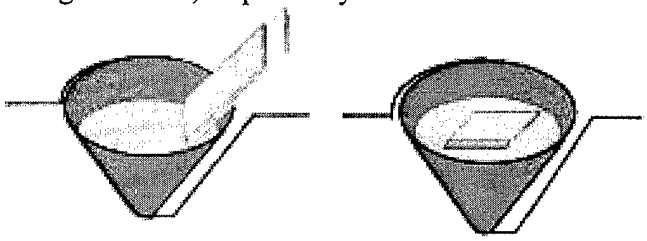

Figure 4. Schematics of experiment with bulk pool of gallium melt using an alumina coated conical heater assembly.

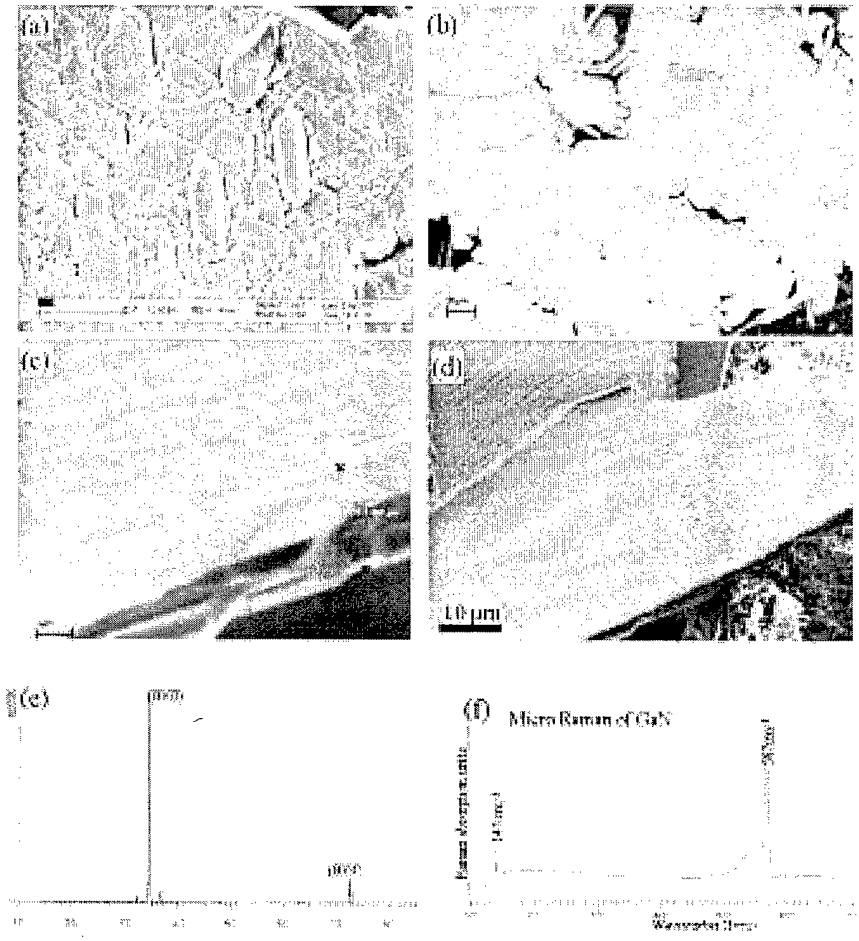

Figure 5. Demonstration of self-oriented growth of GaN films directly on bulk gallium pools: (a) Self-oriented GaN crystals;(b) Part of a large flake of oriented GaN ~ 1 mm^2 in area; (c) & (d)

SEM image showing joining and self-orientation of GaN crystals; (e) XRD spectrum showing c-plane orientation; and (f) Raman spectrum with 3.5 cm^{-1} FWHM of E_2^2 mode at 567 cm^{-1} indicating good quality of wurtzite GaN.

2. Nucleation and early stage growth of GaN from molten gallium

2.1. Self-spreading phenomena of nitrogenated gallium

The amorphous quartz substrates were ultrasonically cleaned in acetone and dried using Ar gas. Ga films between 20-500 μm thick were applied onto the quartz substrates. The chamber was baked, pumped to base pressure and cycle purged with N_2 to remove any residual oxygen and moisture. Next, the gallium film was exposed to N_2 plasma, and the substrate temperature was ramped up from room temperature to 950°C in half an hour using a Boralectric™ heater. While increasing the temperature, the original gallium film agglomerated into droplets on the substrate with a considerable size distribution. These gallium droplets started to spread after exposure to atomic nitrogen at around 950°C. Gradually, the nitrogenated gallium melts covered the substrate and a thin, gray colored solid film formed on top of the molten gallium layer. The spreading of gallium melts is found to be critical in forming smooth textured films.

To study the spreading phenomena of gallium over the substrate during the nitridation, we conducted a series of experiments to find out the wettability of gallium over different substrates under different conditions. Whenever a gallium droplet was placed onto a quartz substrate at room temperature in air, it remained intact and did not spread. A nice gallium film could be made out of the droplet by smearing the droplet using another piece of glass. In a vacuum chamber, the film gradually broke up with an increase in the substrate temperature and agglomerated into several droplets above 600 °C, and remained intact even when cooled back to room temperature under vacuum. The same phenomena happened under both N_2 and H_2 atmospheres. These results indicate that pure gallium melts do not wet the quartz substrates. However, under the presence of oxygen, Ga wets quartz substrates fairly well probably due to the affinity between gallium oxide and oxide substrates. This phenomena is also supported by the fact that a gallium film could not be formed on polycrystalline AlN, or pyrolytic BN substrates by smearing the droplets easily.

Another experiment involved the placement of gallium droplets onto quartz substrates and exposing them to nitrogen plasma to investigate the spreading phenomena under atomic nitrogen atmospheres. Fig. 6(a) shows the spreading of the gallium over the substrate. A layer of gallium nitride was found on the quartz substrate in the region outside of the droplet from the cross sectional images shown in Fig. 6(b). On top of this gallium nitride layer, there was another layer of gallium with decreasing thickness away from the original gallium droplet.

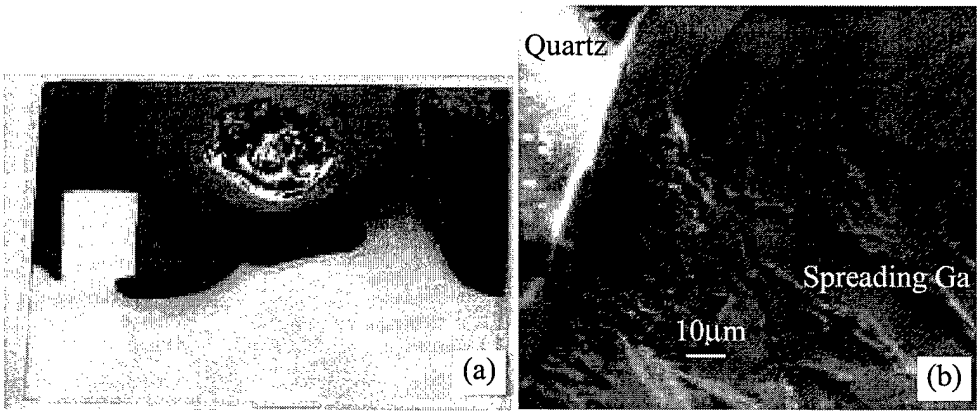

Figure 6. (a) Spreading of gallium over quartz substrates seen with dark grey colored GaN/Ga film over entire region around shiny Ga/GaN pool. (b) Cross sectional SEM micrograph of the region near the original Ga shows the GaN formation and further Ga flow on top.

2.2. Nucleation Kinetics During Early Stages of Growth

It was difficult to maintain a uniform Ga film thickness in determining the nucleation kinetics due to agglomeration during temperature ramp-up and subsequent spreading with exposure to atomic nitrogen. Therefore, gallium droplets with sizes varying from 20 μm to 5 mm were used in an ECR-MW plasma reactor (shown in Fig. 7 (a)).

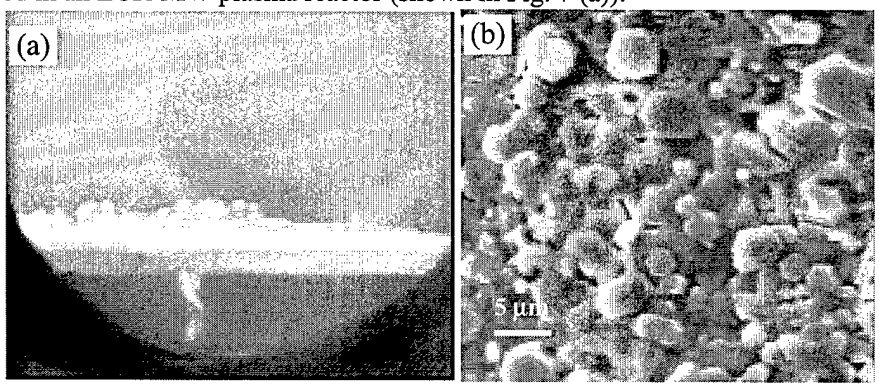

Figure 7. (a) Plasma nitridation of gallium droplets of different sizes heated from below (b) Horizontally oriented GaN hexagonal platelets of varying sizes on 2.1mm gallium droplet

The domain size and nucleation density were calculated from the top view micrographs shown in Fig. 7(b). In Fig. 7(b), both primary and secondary growth events can be seen. The primary nuclei were identified using cross-sectional samples of the GaN formed on Ga droplets. The counting statistics included only the crystals from GaN layers directly on top of Ga. It was difficult to distinguish grain boundaries in the polished, cross-sectional images using either optical microscopy or SEM (Fig. 8(a)). The polished

samples were then treated in 1M KOH for 12 hrs in order to reveal the grain boundaries, as shown in Fig. 8(b). The micrographs of treated samples show parallel alignment of similarly sized individual GaN crystallites, indicating that the nucleation occurred spontaneously from the gallium melt.

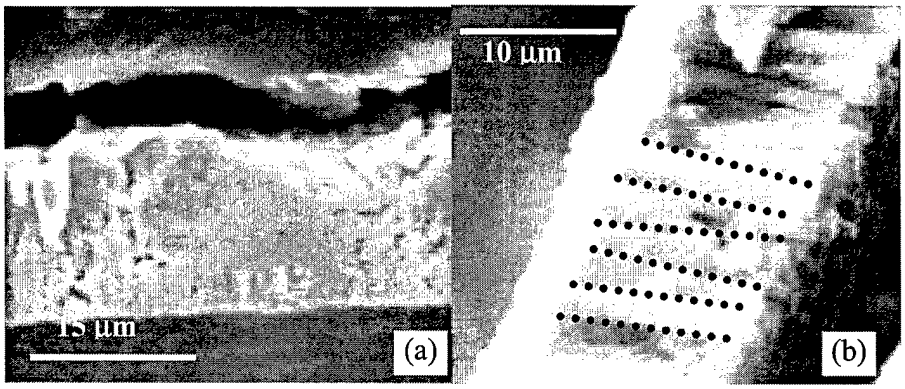

Figure 8. (a) As polished cross-sectional GaN sample does not reveal the individual grain boundaries; (b) Cross-sectional GaN sample after KOH treatment reveals grains that are parallel with approximately the same dimensions.

A strong correlation was also observed between the gallium droplet size and the GaN crystal domain size, as shown in Fig. 9. The above observations indicate that the nucleation of GaN from molten gallium occurs in the bulk and not on the surface. The behavior of the nuclei size with respect to the gallium droplet size follows a sigmoidal curve. At small droplet sizes (20-600 microns), the nuclei size increases with a small slope. Between droplet sizes ranging between 1-2.5 microns, the increase is more pronounced. Beyond 2.5 microns, the nuclei size effectively remained constant. Further experiments are being performed at higher droplet diameters to confirm the trend observed.

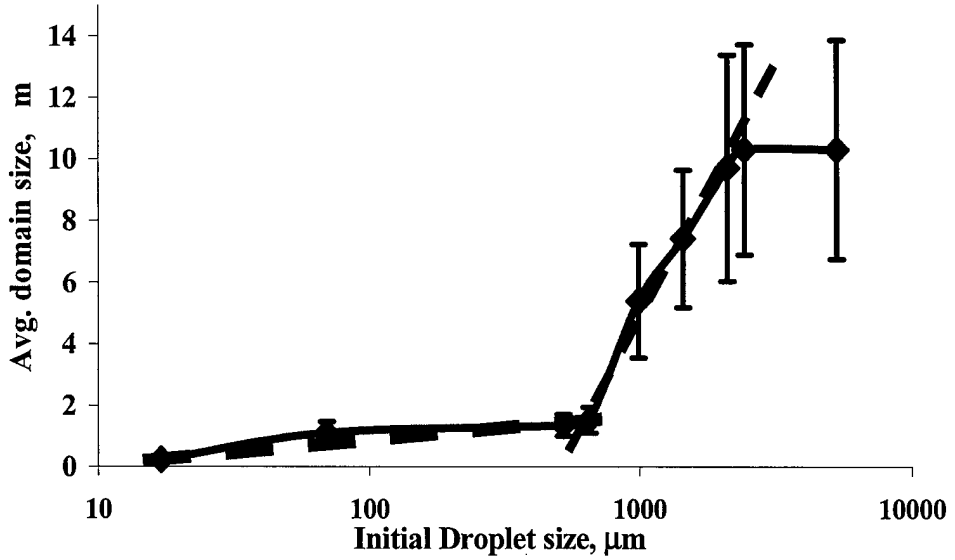

Figure 9. Plot indicates an increase in average domain size with increase in initial droplet diameter.

Estimation of the nucleation density from SEM micrographs clearly shows an exponential dependence on the droplet size, as shown in Figure 10.

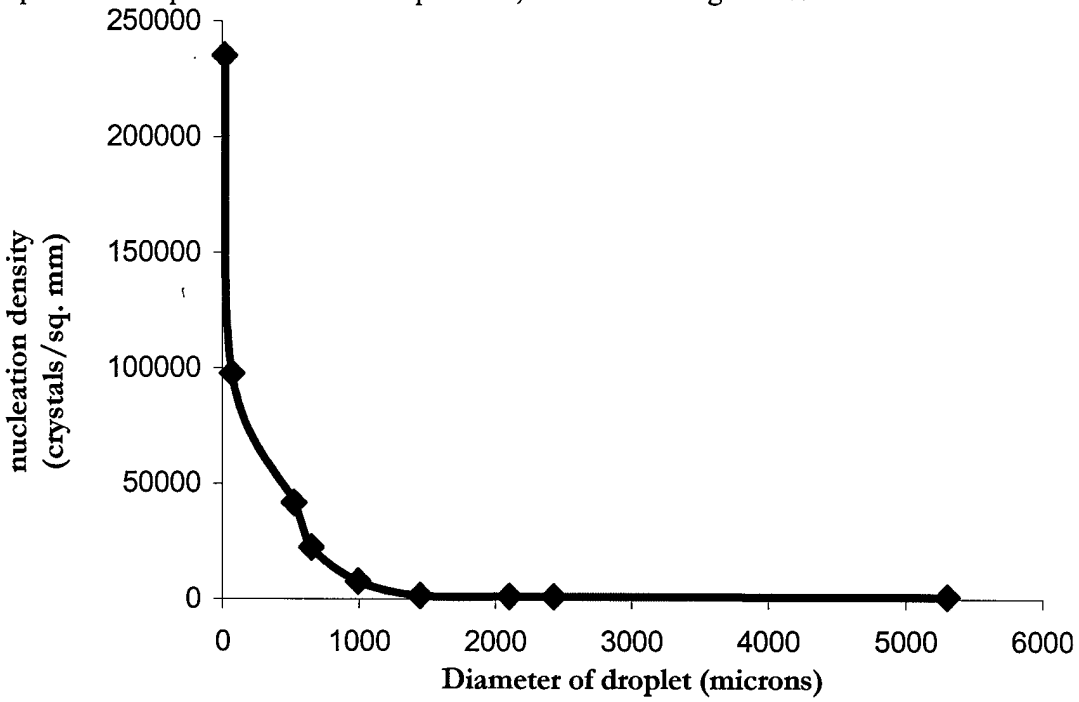

Figure 10. Nucleation density decreases exponentially as the diameter of the of the gallium droplet is increased.

If we assume that the GaN nucleation follows bulk nucleation, the critical nuclei diameter can be estimated using classical nucleation theory:

$$d_c = \frac{4\sigma\Omega}{RT\ \ln(c/c^*)} \qquad (1)$$

Where, σ is the interfacial energy, Ω is the molar volume and c is the concentration of dissolved nitrogen and c* is the equilibrium concentration. The equilibrium solubility, c*, of nitrogen in gallium melts could easily be determined using thermodynamics and is expected to be extremely small (<0.01 at%). However, the estimation of the actual nitrogen concentration, c, present in gallium melts during nitridation is difficult.

We qualitatively determined the correlation between the critical nucleation diameter and the radius of the gallium droplet.

From (1) we know that,

$$d_c \alpha \frac{1}{\ln(c)} \tag{2}$$

The concentration of monatomic nitrogen, c, within a gallium droplet is correlated with the droplet diameter using the following approximations:

1. The mass flux of atomic nitrogen, J, from the vapor phase is uniform. The surface diffusion is not limiting on molten Ga since it is faster than bulk diffusion.
2. The incubation time scale for the nuclei formation is similar in all droplets, and is much larger than the time scale required in achieving a steady state concentration.
3. We also assume that each droplet is a CSTR; hence the bulk concentration in the molten gallium droplet is uniform.

Then, the relation between the concentration, c, and the mass flux, J, can be expressed as the following:

$$c \alpha J \frac{surface\ area\ of\ droplet}{volume\ of\ droplet} \tag{3}$$

$$\Rightarrow c \alpha J \frac{2\pi r^2}{\frac{2}{3}\pi r^3} \quad \Rightarrow c \alpha \frac{1}{r} \tag{4}$$

From (1) and (4), we get

$$d_c \alpha \frac{1}{\ln\left(\frac{1}{r}\right)} \tag{5}$$

$$\Rightarrow d_c \alpha \ln(r) \tag{6}$$

The experimental relationship between crystal size and the droplet diameter is a linear as seen in the central region of Fig. 7, which is consistent with the above analysis based on the bulk nucleation concept. However, the sigmoidal behavior is not completely explained by this equation, and we are currently investigating the origin of the sigmoidal behavior. For droplet diameters between 20μm - 1mm, the domain size of the GaN crystals increases slowly, but for droplets with diameters between 1mm-2.5mm, the increase in domain size is drastic. At much higher droplet diameters, preliminary results suggest that the domain size saturates. Further data points are required to confirm the domain size where bulk saturation effects take place and surface phenomena dominate for the nucleation process, i.e., beyond certain thicknesses of Ga used, the atomic nitrogen diffusion in the bulk of the Ga becomes the limiting factor. The data suggest that beyond certain thicknesses of Ga films, the nucleation process is independent of the Ga film thickness. Below such Ga thicknesses, the nucleation of GaN seems to be a bulk phenomenon and not a surface phenomenon.

The nitrogen plasma chemistry in our ECR reactor was modeled using SAMPR (licensed from Dr. Meyya Meyyappan of NASA Ames). The concentration of the active nitrogen is found to reduce as the pressure of the reactor increases, as shown in Fig. 11. Hence, we are currently performing experiments at various pressures for similar droplet sizes to determine the correlation with the active nitrogen concentration in the gas phase.

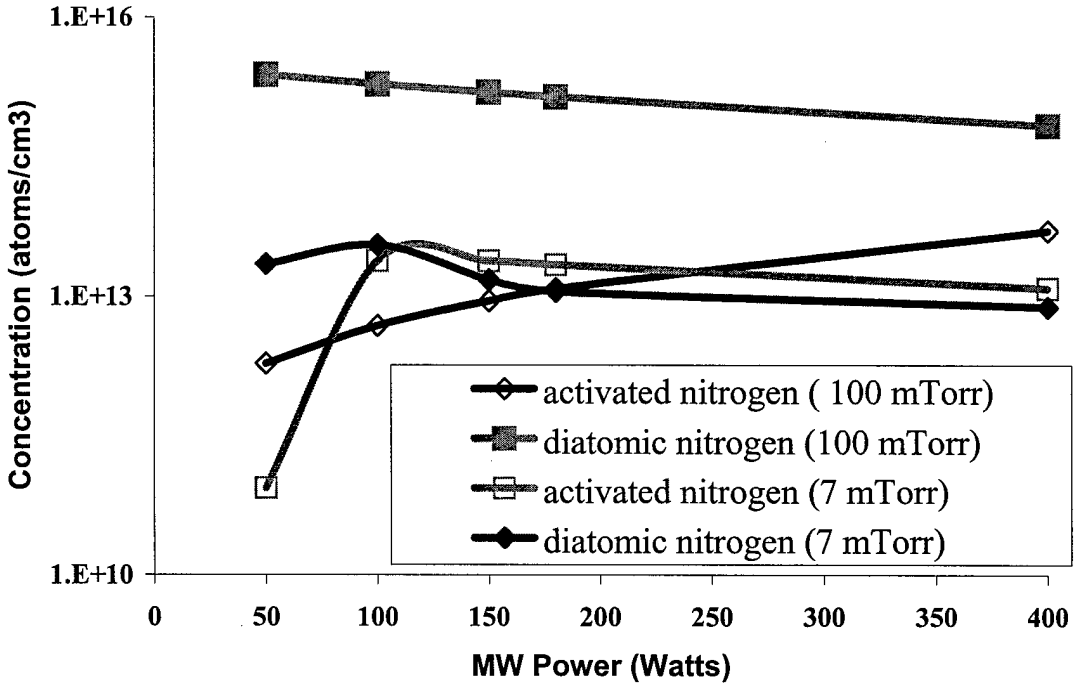

Figure 11. SAMPR calculations predict that the active nitrogen concentration decreases as the pressure of the reactor increases.

3. Mechanistic studies of GaN crystal growth

3.1 Morphologies of GaN crystals

The morphology of the resulting GaN single crystals during our nitridation process plays an important role during self-oriented film formation. The ideal desired morphology of individual GaN crystals is c-plane aligned platelet shaped crystals perfectly joining during coalescence in the early growth stages. Typically, plate-like and needle-like pyramidal prisms are the most commonly observed morphologies of GaN single crystals. For high pressure solution growth techniques, the platelet-like, and needle-like morphologies were attributed to low and high supersaturation of nitrogen, respectively[19-20]. Other reports suggest that the plate-like morphology occurs during gallium rich conditions, and the needle-like morphology is favored when nitrogen rich conditions are used [21-23]. However, it is unclear how one defines nitrogen rich conditions, i.e., the level of dissolved nitrogen. In our low-pressure bulk synthesis using atomic nitrogen, several unusual morphologies of gallium nitride crystals were observed.

3.1.1. Hollow platelets

The dissolution of atomic nitrogen at high temperatures (> 950 C) into molten Ga resulted in the wetting of the melt onto the substrate. The flow caused during wetting caused the GaN crystals to be (0002) plane oriented on top of the Ga layer. Most of the GaN crystals were micron sized and plate-like (Fig.12 (a)). Vertically oriented hollow and irregular platelets were also observed in some regions when unevenly heated from the bottom using an alumina-coated tungsten coil heater (Fig.12 (b) and Fig 13). There were several narrow struts between the two adjacent layers of the platelets. Some of these struts were at the edge of the platelets. A layer-by-layer growth mode was also clearly shown on the top surface of both layers of the platelets.

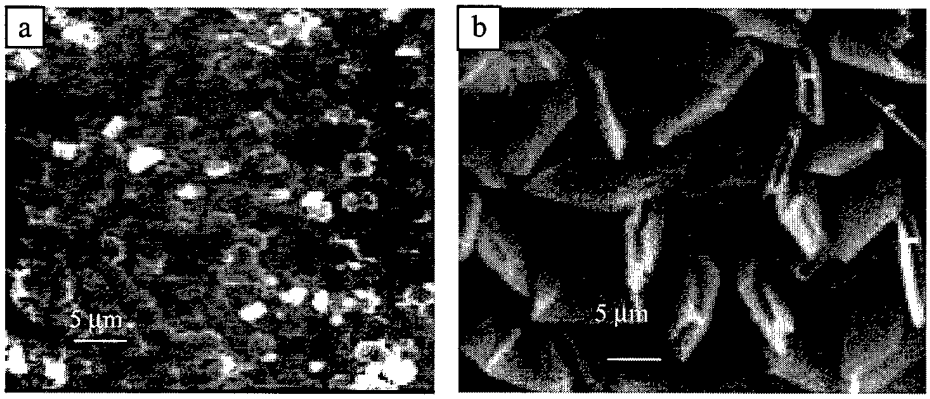

Figure 12. (a) GaN platelets crystals (b) Standing hollow platelets crystals

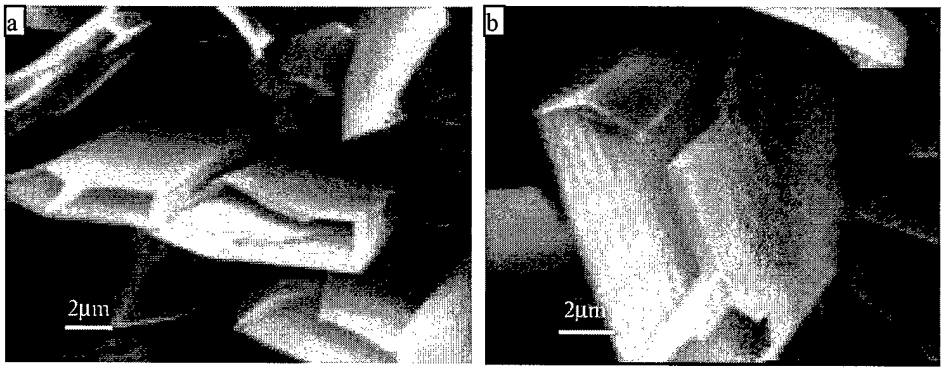

Figure 13. Standing GaN hollow platelets with struts between two layers

It is well known that convection in the melts influences crystal growth kinetics, compositional homogeneity, nucleation and morphological stability [24]. A preliminary analysis showed that convection does exist due to the non-uniform heating caused by this particular heater [25]. The solute concentration on the crystal surface varies along the surface even without convection. Convection, especially the strong Marangoni convection present in our experiments [25], made the platelet-shaped crystals to align vertically such that the edge plane of the hexagonal platelet is parallel to the substrate. Stable layer-by-layer growth can only occur if the step formation is slower than step propagation, but step generation usually happens where the supersaturation is the highest. Steps form primarily at the edge of crystals due to a high solute concentration at the two side facets where the flow is greater than that at the center of the crystal. The strong convection flow fields could affect the kinetics, and step propagation could get slower than step generation. The

formation of the top layer was possible due to the stable growth mode when the convection was not strong. In this manner, the evolution of hollow platelets with narrow struts between two layers is envisioned.

3.1.2. Hollow crystals

Several crystals with depressions in the center of the top face are shown in Fig. 14. The depressions exhibit varying depths and irregular shapes for different crystals. Fig 14(b) shows a close look at one shallow depression. A layer-by-layer growth mode is clearly seen. The layers are trying to propagate to the center from the edge, and the newer layers on the top surface stop further away from the center. Therefore, the depression has a shape resembling a cone.

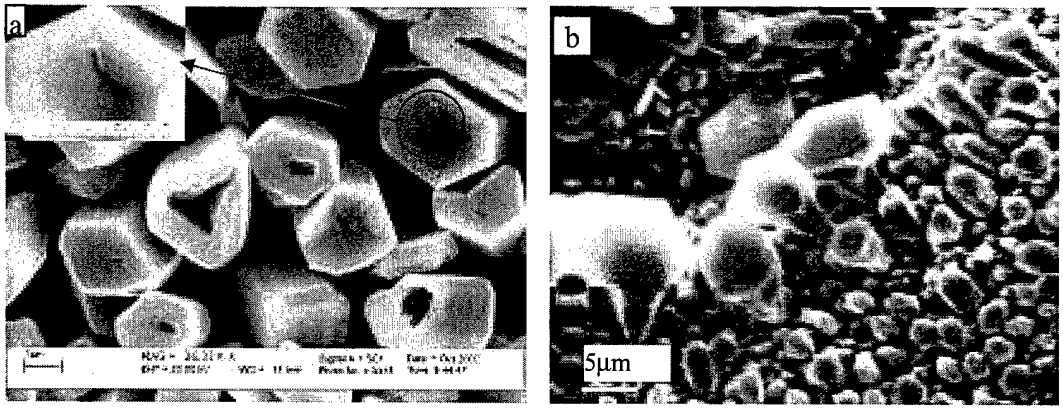

Figure 14. Hollow hexagonal GaN pillars. Inset in (a) is a high magnification image of the crystal shown in (a) as indicated by the arrow. (b) hollow conical platelets

Ga wets GaN very well at high temperatures [26]. When the GaN crystals reached a certain size and were not fully immersed in the liquid gallium, the liquid gallium wetted the crystals and formed a thin gallium layer on the surfaces of the crystals. Simultaneously, GaN growth occurs using nitrogen supplied from the gas phase. Because the top surfaces of these crystals were further away from the surface of the liquid gallium due to the growth of crystals or the consumption of gallium, it became more difficult for the gallium to creep up and go further towards the center of the top faces. Gradually, it left an inverted cone-shaped depression. This phenomenon is further supported by observations of some crystals whose depressions are further away from the side closest to a gallium pool. (See Fig.14(b))

3.1.3. Star-shaped crystals

Six-arm, star-shaped crystals were also found in experiments using 10:1 N_2:H_2 (Fig.15). Most of the star-shaped crystals have a pyramid top (Fig. 15(a)), but some of them have a flat yet rough top surface (Fig. 15(b)), or pitted surface (Fig. 15(c)). Seen from the side (Fig. 15(d-f)), the star-shaped crystals with pyramid tops have a star-shaped column at the bottom. The angles of the six-arms were measured from the SEM pictures and it was found that they are not the same, varying from 70° to 110°, but most of them

are around 90°. Such measurements are not completely accurate since the crystals are three-dimensional while the micrographs are two-dimensional, but it seems that the star-shaped crystals do not have six-fold symmetry.

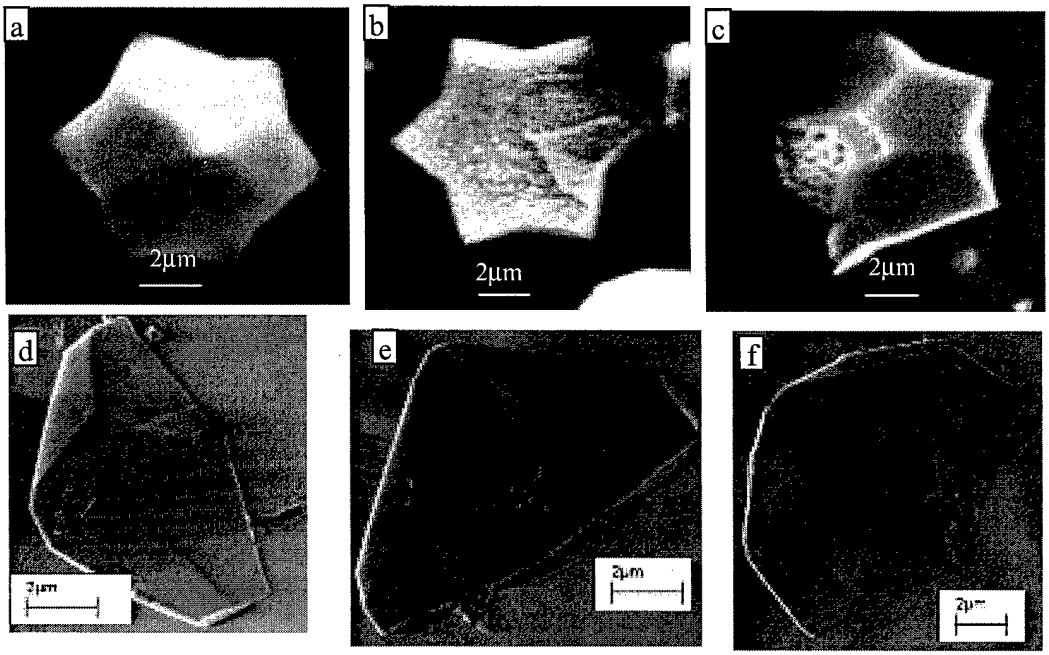

Figure 15. Different star-shaped GaN crystals

Geometrically, many hexagonal stars are possible from a unit hexagonal lattice. There are two basic types of equilateral stars from which the six arms originate: edge (Fig. 15(1)) and corner (Fig. 15(4)). Shown in Fig. 15(2,3,5,6) are four different six-fold symmetrical stars bounded by the same group low index (maximum is 3) planes. Among them, (2) and (5) with angles of 60° for the arms are bounded by $\{11\bar{2}0\}$ planes and $\{20\bar{2}0\}$ respectively; (3) and (6) are bounded $\{21\bar{3}0\}$ planes but they have different arm angles of 82° and 98°, respectively. Considering the side faces of the pyramid top, they could be $\{11\bar{2}n\}$ for the form of the star shown in Fig. 16(1) and $\{10\bar{1}n\}$ (n=1, 2) for the form shown in Fig. 16(4), respectively. Comparing the configurations of the star-shaped crystals, it was found that they are more like the star in Fig. 16(3) and should have side pyramidal faces of $\{10\bar{1}n\}$ since $\{10\bar{1}n\}$ planes showing up in many kinds of GaN crystal growth but $\{11\bar{2}n\}$ only showed up in lateral epitaxial overgrowth (LEO) under certain conditions [27]. This is further supported by the angle between the side pyramidal face and base plane shown in Fig. 15(e). They are around 42° to 46°, which are very close to the angles between $\{10\bar{1}2\}$ and $\{0001\}$, 43°.

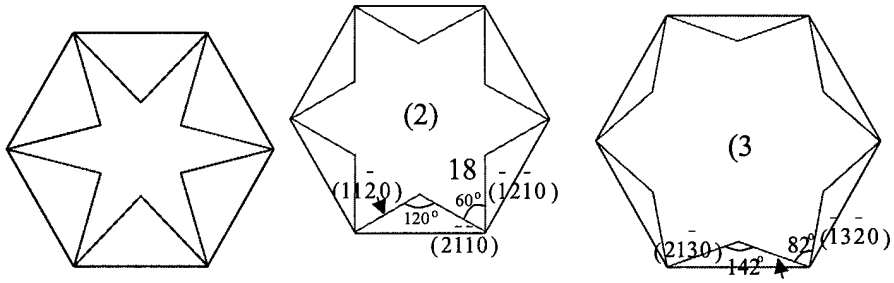

(1)

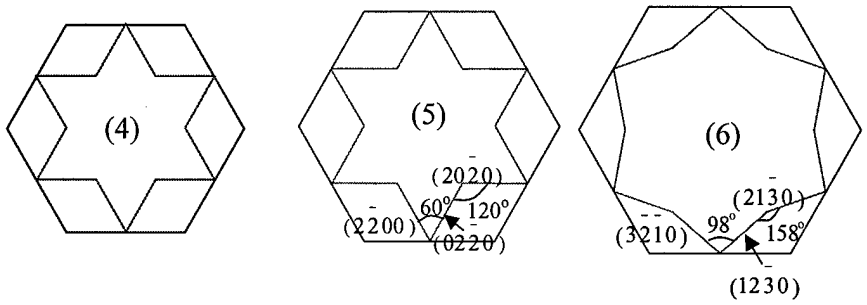

Figure 16. (1)&(4) The two basic kinds of stars with 6-fold symmetry from a hexagon, (2,3,5,6) Four different kinds of six-fold symmetrical stars bound by low index planes (≤ 3)

The planes that grow slowest after the faster growing planes and eventually disappear from the crystal determine the morphological form of the crystal. It is known that the growth rate increases with increases in attachment energy [28]. Hartman calculated the attachment energy of hcp crystals and found that the growth rate of some planes has the following relationship [28]: $R\{11\bar{2}0\} > R\{10\bar{1}1\} > R\{10\bar{1}0\} = R\{0001\}$. This explains why hexagonal platelets and prisms formed by $\{10\bar{1}0\}$ planes and $\{0001\}$ planes are mostly found in GaN crystal growth. The planes shown in Fig. 16 cannot be explained completely using the above theory. The presence of those high index planes and the rough surface of some crystals are possibly due to the presence of H_2. GaN is believed to decompose under high temperatures [29], and the adsorption of active hydrogen in the plasma on the surface of GaN crystals promotes the decomposition of GaN and might stabilize those surfaces. A Monte Carlo simulation algorithm is currently being formulated to simulate individual GaN crystal growth to gain further insight.

3.2. Sequential growth of self-oriented GaN film

SEM images of intermittent growth experiments in Fig. 17 clearly show the growth and coalescence process of the GaN platelets on top of molten gallium. A layer of molten gallium can be seen from the cross sectional SEM micrographs in Fig. 18. GaN platelets grew with both basal attachment and top growth through liquid phase epitaxy before they fully coalesced to form a film. This growth mechanism is justified since the atomic nitrogen could dissolve into gallium and diffuse to the surface of the GaN platelets. Also, a layer of liquid gallium could flow over the GaN platelets due to good wetting properties and develop liquid phase epitaxy. Cross sectional TEM analysis (discussed later) also substantiates this possible growth mechanism. The basal growth almost ceased after the coalescence since the overlaying GaN film hinders dissolution of atomic nitrogen.

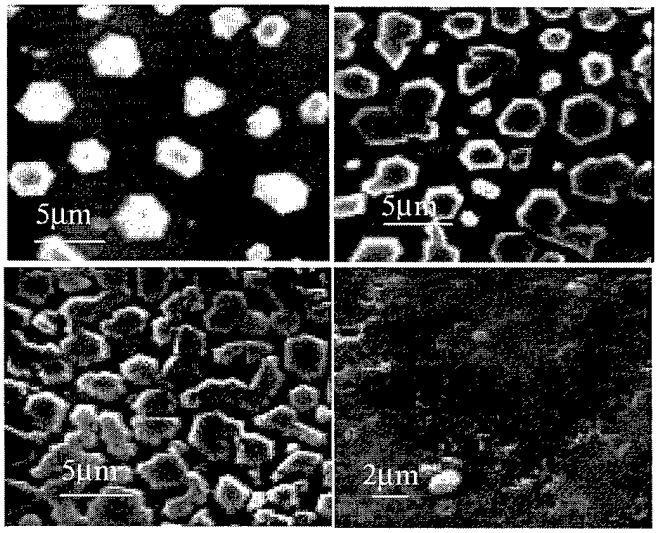

Figure 17. Plan-view SEM images of sequential growth of oriented GaN on top of gallium

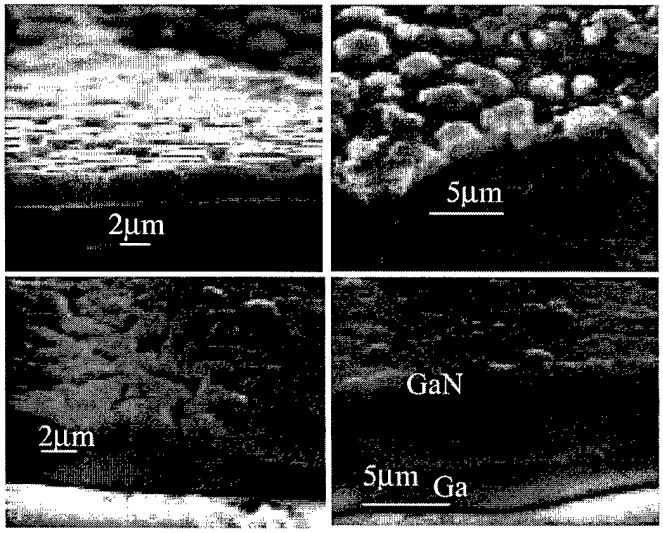

Figure 18. Cross sectional SEM micrographs of sequential GaN oriented on molten gallium

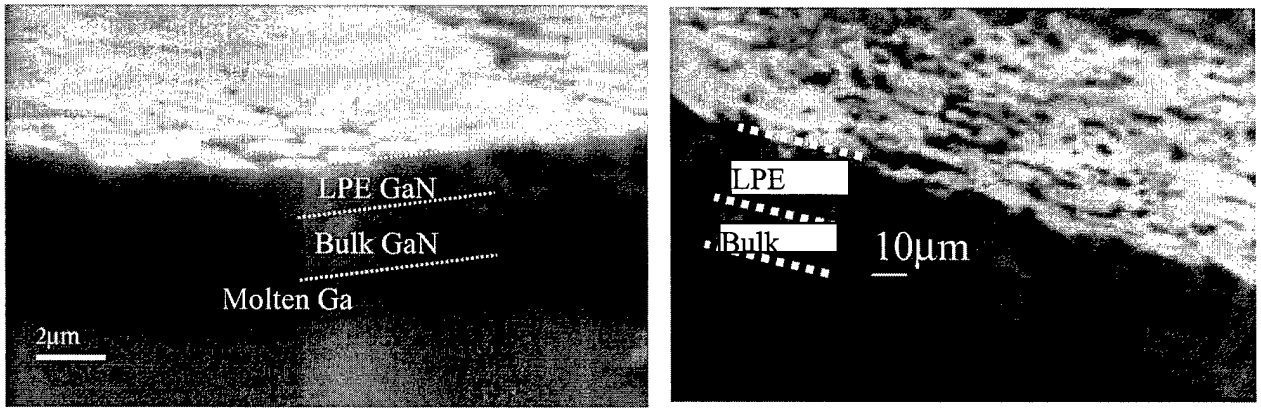

Figure 19. SEM micrograph clearly shows the demarcation between bulk growth and epitaxial growth of GaN on molten gallium

After film formation, further growth occurs through liquid phase epitaxy with the Ga supply from below by flowing through the cracks, fissures and other discontinuities in the GaN film. The evidence of two growth modes indicated with dashed lines is shown in Figure 19.

4. Large area self-oriented GaN film growth on molten gallium

4.1 Orientation Analysis of GaN Films

The spreading of gallium melts was found to be critical in forming the smooth textured films shown in Fig. 20. An X-ray diffraction spectrum of the GaN film on top of gallium from the experiment with spreading shows only reflections of (0002) and (0004) planes of wurtzite GaN (Fig.21(a)), indicating good c-plane orientation. The XRD spectrum of the GaN crust on top of non-spreading gallium melts in Fig. 21(b) shows all the characteristic peaks of wurtzite GaN. The cross-sectional SEM image of the sample that exhibited a smooth textured GaN film clearly indicates the presence of a layer of gallium between the substrate and the GaN film as shown in Fig. 22(a). A representative image is shown in Fig. 22(b) for GaN films without the presence of any molten Ga buffer layer. The difference between Figs. 22(a) & (b) indicates that crystals grown on molten Ga buffer layers self-assemble to form an initial smooth textured film.

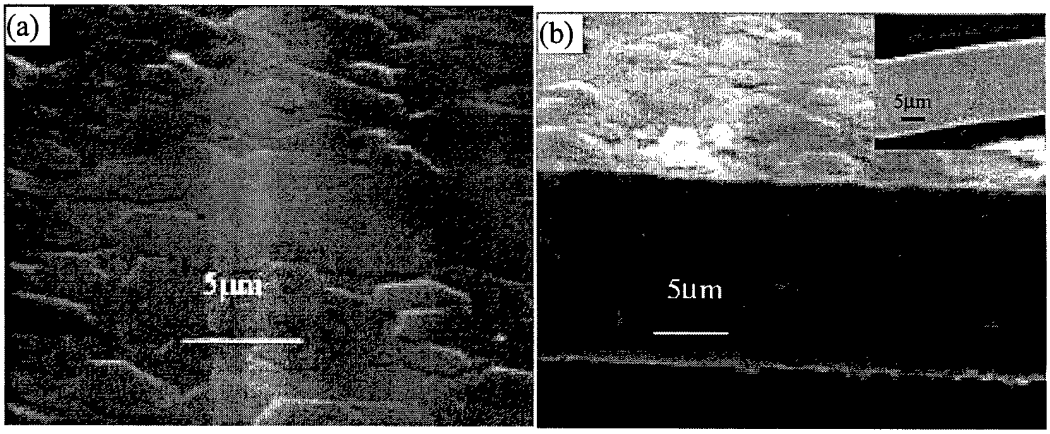

Figure 20. Representative SEM images of a smooth, c-plane oriented GaN film (a) plan view (b) cross section view, inserted is a cross sectional TEM sample after polishing.

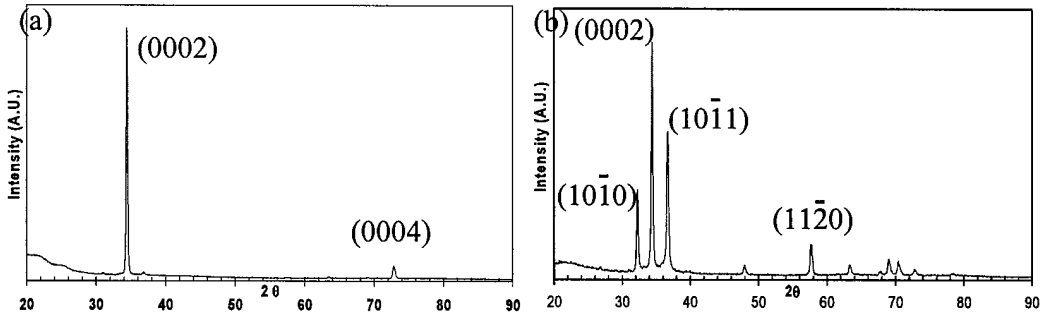

Figure 21. XRD spectra of GaN films obtained under two different wetting conditions of molten Ga: (a) Ga wets the substrate during nitridation experiments and (b) Ga partially wets the substrate during nitridation.

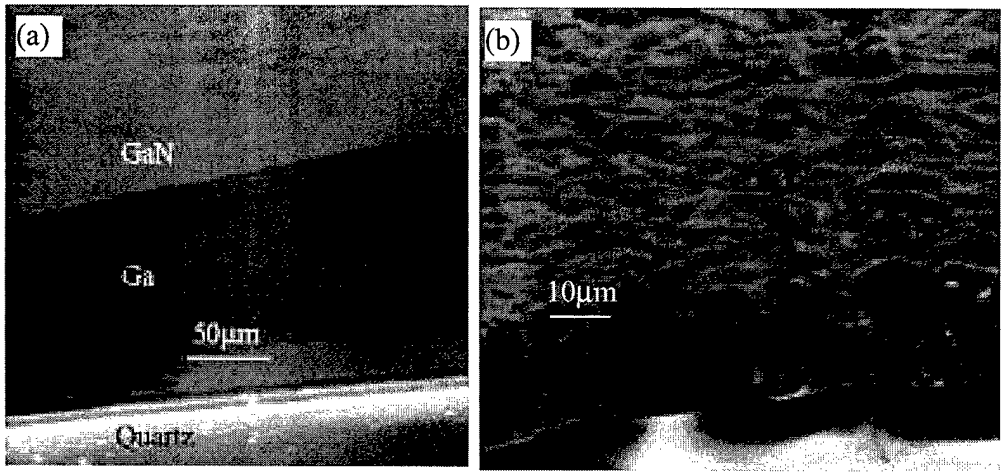

Figure 22. The SEM images of two different GaN films: (a) GaN grown directly on top of flattened Ga and (b) GaN grown directly on the amorphous Quartz substrate without the Ga buffer layer.

Raman spectra were taken using a 632.8nm HeNe laser at room temperature with a Renishaw InVia Raman microscope. The spectra with the laser beam parallel to the c-axis under which only E_2 and A_1 (LO) modes are allowed for hexagonal GaN [30] are shown in Fig. 23. The spectrum of GaN grown on top of gallium shows the characteristic peaks of E_2^1 at 143 cm^{-1}, E_2^2 at 567 cm^{-1} and A_1 (LO) at 738 cm^{-1}. The A_1 (LO) peak for the GaN grown directly on a quartz substrate was missing. The disappearance of A_1 (LO) mode is believed to be the result of plasmon-phonon interactions with electron concentrations exceeding 10^{19} cm^{-3}[31], which come from the diffusion of oxygen from the quartz substrate.

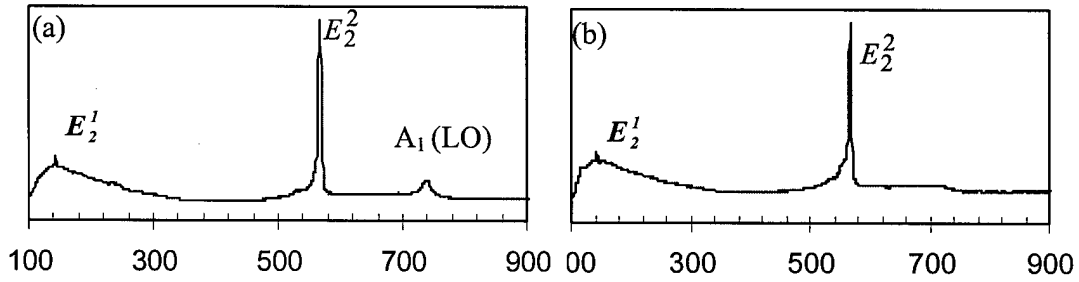

Figure 23. Raman spectra of (a) GaN on gallium, (b) GaN grown directly on quartz substrates, the absence of A_1 (LO) peak for GaN on quartz indicating high electron concentration from oxygen diffusion.

4.1.1. XRD analysis over large area film

To acquire both phase and orientation information of textured GaN films, XRD texture analysis was performed using a Bruker GADDS system with an area detector.

The x-ray source spot size of the system is a few mm and the penetration depth is about 100μm. The scans taken using the area detector are read as three-dimensional plots, where the horizontal direction in conical cross-sections represents 2θ, the vertical direction χ is the tilt with respect to the plane represented by the X-ray source and the detector. The color contours represent the intensity of the peaks. Figure 24(a) shows the plot centered at 2θ=34.6°, χ=90° for 5mm×5mm GaN free standing flakes on top of Ga. The χ integration of the (0002) reflection line from the plot in Fig. 24(a) is shown in Fig. 24(b). There is a small reflection of (10-11) along with the strong (0002) reflection of wurtzite GaN. The presence of the (10-11) reflection is attributed to the presence of some skewed crystals in the films as shown in the inserted SEM images. (See Fig. 24(a)). The 2θ integration of the (0002) reflection line in Fig. 24(c) indicates the tilt of the crystalline domains with respect to the normal, c-axis, which is about 2.2° determined from the full width at half maximum (FWHM) of the curve.

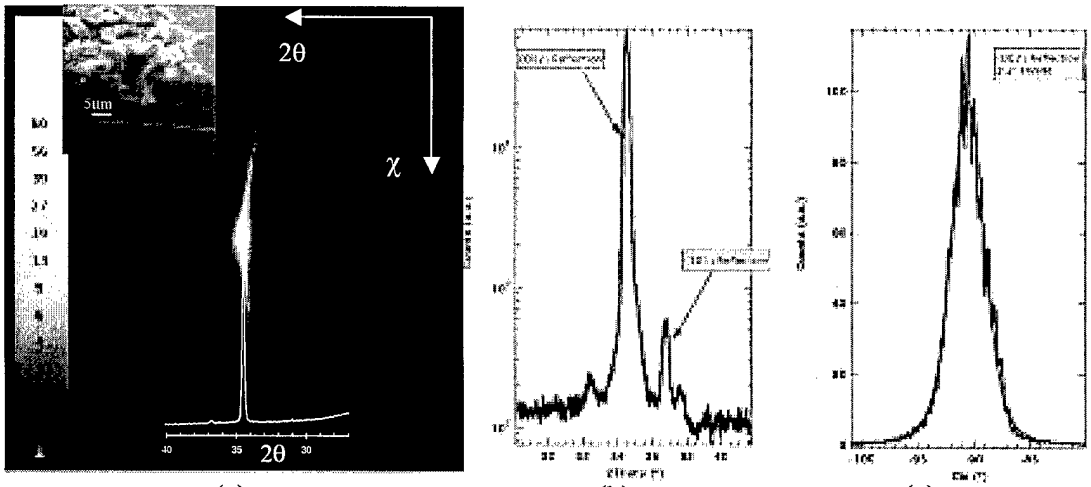

(a) (b) (c)

Figure 24. (a) XRD texture analysis of a 5mm×5mm free standing GaN flake; (b) χ integration of the (0002) reflection line indicates strong preferential orientation; (c) 2θ integration of the (0002) reflection line showing a FWHM of 2.2°.

4.1.2. TEM studies of orientation between individual crystals

Fig. 25 shows a bright field TEM image from a cross-section of the GaN films grown directly on Ga. The image was taken with the 2nd grain oriented with a $<11\bar{2}0>$ zone axis. The contrast observed clearly shows the existence of grain boundaries with misorientation between two adjacent crystals. Columnar growth of GaN crystals could be seen and no dislocation crops are found inside individual grains. The contrast observed shows the existence of slight misorientations between adjacent crystals. However, the cross-sectional image shows contrast for possibly two different growth modes, growth

downwards with basal attachment and another growth mode using epitaxy from the top, as indicated in Fig. 25. The alignment of crystals seems to be set during film formation in the initial stages of nucleation and growth, which probably occurs at the region indicated by the dashed line. For growth upwards, Ga was supplied to the top through the cracks and holes within the GaN film and spread quickly over the entire region of the top surface. On the other hand, the basal growth seemed to stop after a few microns of growth as evidenced in several experiments with different nitridation time scales. Note, each of the successful experiments had Ga remaining at the bottom of the self-oriented GaN film.

Inserted is a selected area diffraction pattern of the 2nd grain in Fig. 25. The diffraction pattern indicates a single crystal pattern with a zone axis of $[11\bar{2}0]$. The (0001) diffraction spot is seen in the pattern due to double diffraction resulting with the $[11\bar{2}0]$ zone axis. This was also confirmed in the dark field imaging analysis of the (0001) diffraction spot (not shown here).

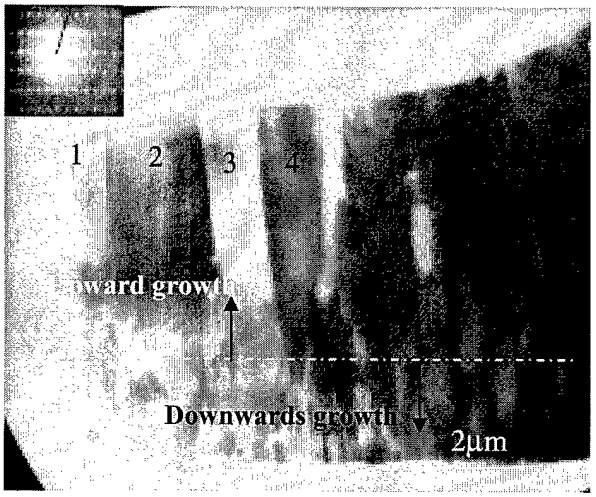

Figure 25. TEM bright field image of a cross-section of GaN film with 2nd grain on ZA $<11\bar{2}0>$ showing contrast resulting from misorientations of few grains. Inserted is selected area diffraction from the 2nd grain on ZA $[11\bar{2}0]$.

Convergent beam electron diffraction (CBED) and Kikuchi lines were employed to quantify the misorientation between the grains. Kikuchi lines are very sensitive to the structural differences between grains [32-33]. The Kinematical SADP Electron Diffraction Simulation program available online at WebEmaps [34] was used to determine theoretical CBED patterns with different X and Y-axis tilts of the grains. The comparison between the simulated CBED patterns using the assumed tilt and twist angles and the experimentally obtained CBED patterns allowed us to determine the mis-orientation among grains within the cross-sectional sample. The CBED patterns were obtained from crystals numbered from 1 to 4 within the cross-sectional sample and are compared with the corresponding simulated patterns. See Fig. 26. The CBED pattern from

grain 1 was taken on a [11$\bar{2}$0] zone axis, and others were taken by just moving the sample to other locations for the convergent beam. The mis-orientations between grain 1 and grains 2, 3 and 4 are 8°, 3°, 9.7° twist in the c-plane, respectively. The tilt of the c-axis in plane (10$\bar{1}$0) for grains 2, 3 and 4 with respect to grain 1 is about 0.2°, -0.4° and 0.1°, which are very small and can be seen from the slightly off-symmetrical CBED pattern.

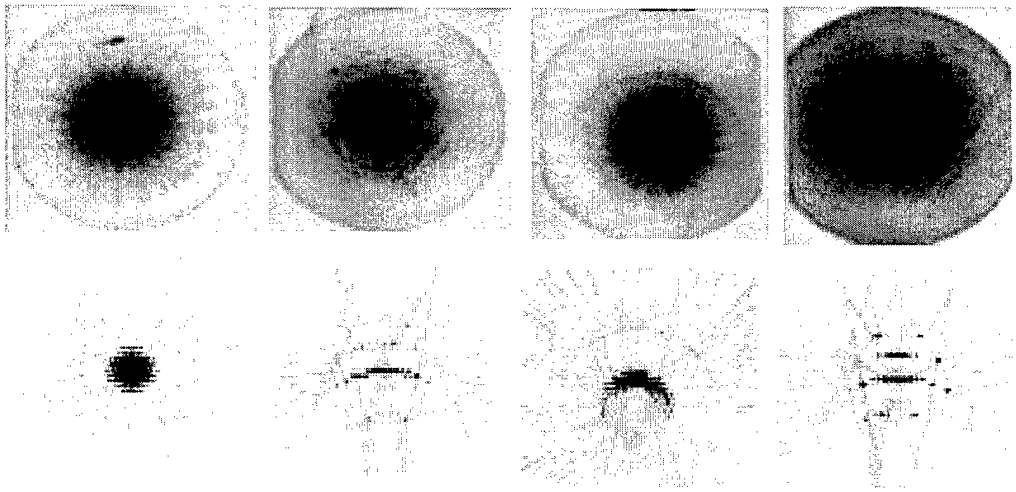

Figure 26. Experimental and simulated kinematical Kikuchi lines using CBED patterns from four grains with the following misorientation: (1) on ZA [11$\bar{2}$0]; (2) 8° twist, 0.2° tilt (3) 3° twist, -0.4° tilt; (4) 9.7° twist, 0.1° tilt; with respect to grain 1.

To further investigate the structure at the boundaries, HRTEM micrographs were taken at two kinds of boundaries. One is a boundary that has almost no misorientation as shown in Fig. 27(a). It was found that there is an intermittent layer of disordered GaN between the two adjacent crystals (Fig. 27(b)). The width of the layer ranges from 2nm to 5nm except both ends of the boundary. The width of the layer at the top of the boundary is around 25 nm, and it was not found at the bottom as shown in Fig. 27(c). The EDX line scan under STEM mode across the boundary in Fig.28 shows the N concentration is apparently lower at the disordered layer. We think the continuous small variation of the growth conditions at the boundary might change the joining of the crystals. The disordered nitrogen deficient layer formed when there was more gallium around the boundary.

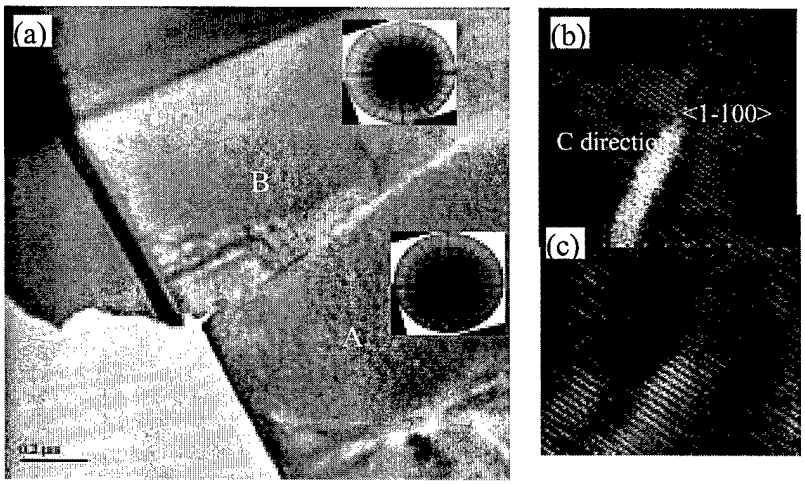

Figure 27. (a) A boundary with almost no misorientation, inserted are the CBED patterns for the grains forming the boundary; (b) HRTEM image of the boundary shows the intermittent disordered layer at the boundary (c) HRTEM images of the bottom part of the boundary shows no disordered layer.

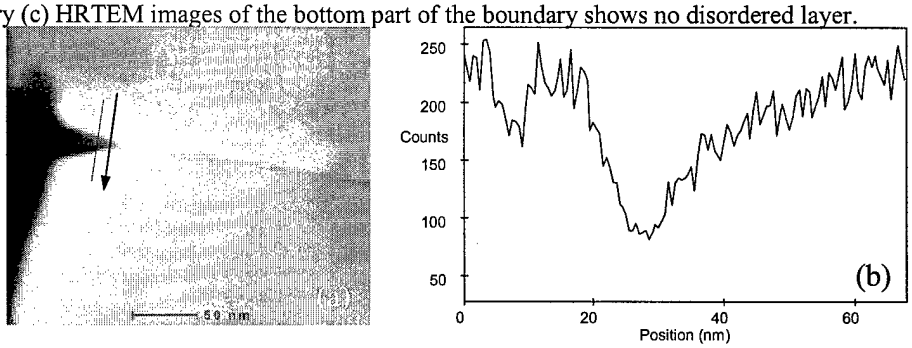

Figure 28. (a) STEM images of the boundary, the red line indicates the region for the EDX line scan; (b) N concentration profile along the boundary shown in (a), dwell time 15s, resolution 0.5 nm

Fig. 29(a) shows the top part of the boundary between grains 2 and 3 shown in Fig. 25 which has a misorientation of 5° twist in the c-plane and 0.6° c-axis tilt. Grain 2 is on zone axis $<11\bar{2}0>$ and grain 3 is off the zone axis as seen in the 1-dimensional lattice showing up in the HRTEM images. The boundary is straight, sharp and no disordered layer was found, while the boundary between grains 3 and 4 in Fig. 25 shows facets at the top region. The angle between the facet and c-plane was found to be around 61°, which is close to the angle between $(1\bar{1}01)$ and (0002).

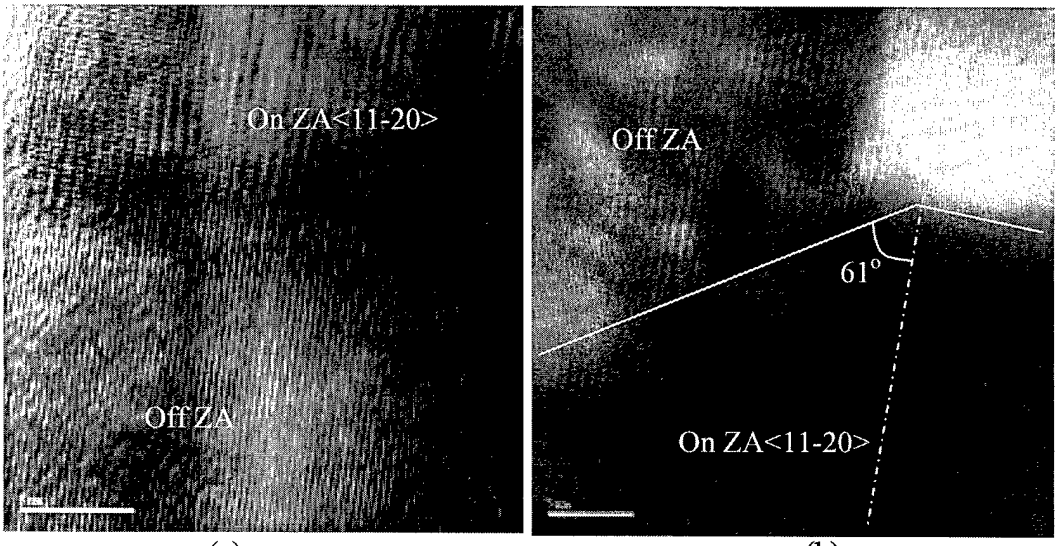

Figure 29. (a) HRTEM images of the straight boundary between grains 2 and 3 shown in Fig. 21 with certain misorientation; (b) HRTEM images of the $(1\bar{1}01)$ faceted boundary between grains 3 and 4 shown in Fig. 22.

In summary, the alternate grains seem to be closely oriented with respect to each other while adjacent grains seem to be misoriented with respect to each other by about 10 degrees. At the same time, SAD yielded a single crystal pattern indicating that there is some sort of self-orientation between crystals within these films with some imperfect attachment and rotational alignment of crystals with respect to each other during growth.

4.2. Large area self-oriented, free-standing GaN flakes

Oriented flakes with areas greater than 1 cm^2 and thicknesses as high as 19 microns have been obtained experimentally. Some of the flakes about 5 microns thick are semi-transparent as shown in Fig. 30. The powder XRD spectrum and χ integration of the (0002) reflection of the flakes in Fig. 24 showed strong preferential orientation.

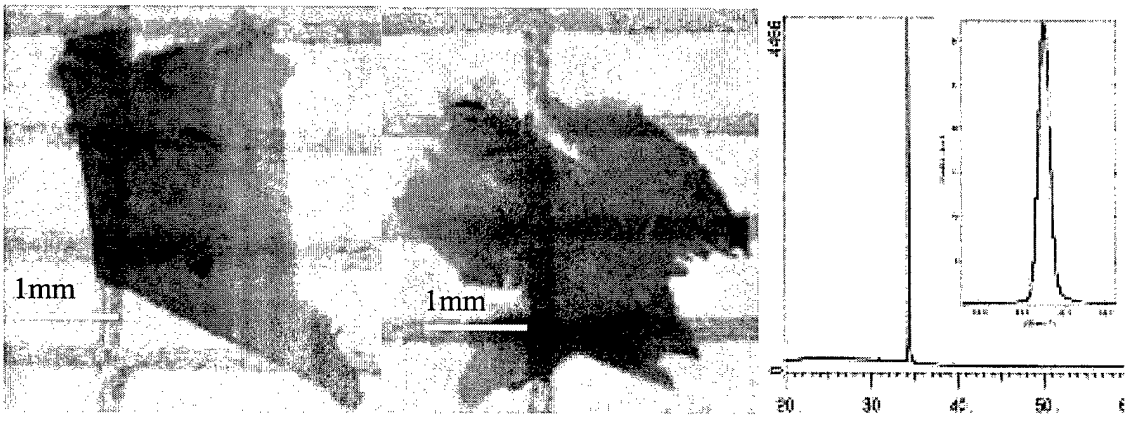

Figure 30. Optical images and XRD analysis of large area oriented flakes

4.3. Rotating substrate stage experiments

We performed preliminary experiments on a custom-built rotating and heated substrate stage, shown in Fig. 31(a), to understand the effect of *in-situ* rotation during GaN synthesis. A thick film (2 mm in thickness) of molten gallium was spread on a quartz substrate and rotated at 500 rpm at nitridation temperatures for 30 minutes. We observe a thin, uniform film of GaN over the entire 1 square inch substrate with a lip on the outer edge about 2 mm thick, as shown in Fig. 31(b). Currently, we have only been able to observe macroscopic uniformity in the resulting GaN film. Further experimentation is currently being performed to obtain single crystal quality GaN films.

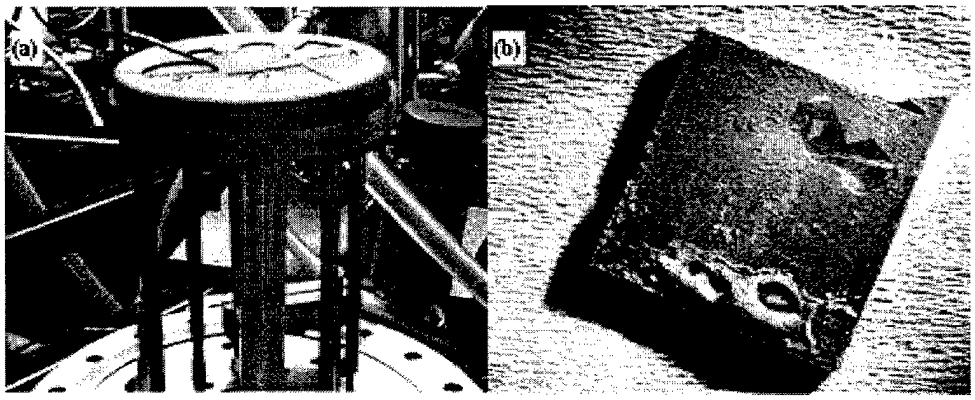

Figure 31. (a) Rotating substrate stage that is simultaneously heated from below during nitridation; (b) 0.25 in quartz substrate coated uniformly with GaN with a gallium lip on the periphery caused by rotation.

5.0 C-plane textured nanocrystalline GaN film

Spin-coating has been widely used to make thin films such as photoresists in microfabrication processes. Liquid gallium (m.p. 29.3°C), despite its high surface tension (700mN/m at 25 °C), wets glass very well at room temperature. Utilizing this property, several micron thick gallium layers were spin-coated onto 2-inch quartz wafers (Fig. 32(a)). A yellowish thin film is formed on the substrate after nitridation in ECR-MW generated nitrogen plasma (Shown in Fig. 32 (b)). Fig. 32(c) shows the size of the crystallites in the film to be around 85nm.

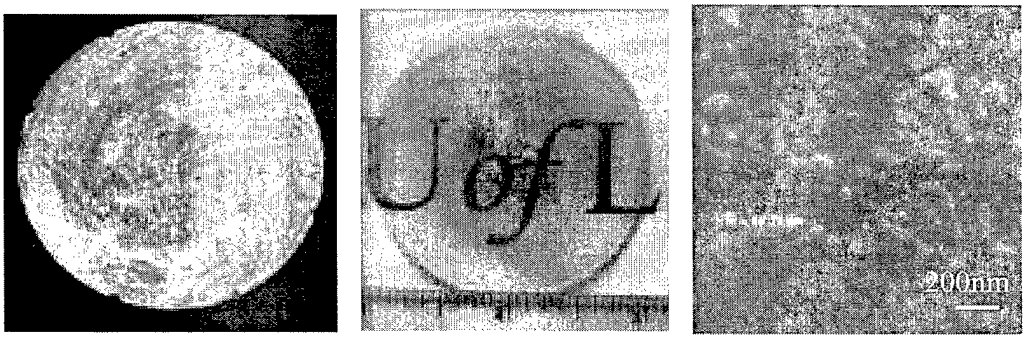

Figure 32. (a) Optical micrograph of spin coated gallium film on 2-inch quartz substrate. (b) Optical micrograph of the as-nitrided substrate.(c) SEM image of Nano-crystalline GaN film showing a crystallite size of 85nm.

Cross sectional TEM images of the film are shown in Fig.33 (a). The thickness of the film is about 500nm. The HRTEM image of the quartz-GaN interface shown in Fig. 33 (b) indicates no epitaxial relationship with the substrates. A band gap of 3.4eV was determined using the Tauc equation [35]: $\alpha^2 = (h\nu - E_g)/(h\nu)^2$ (α is the absorption coefficient) from the UV-Vis spectrum of the film. (Fig.34)

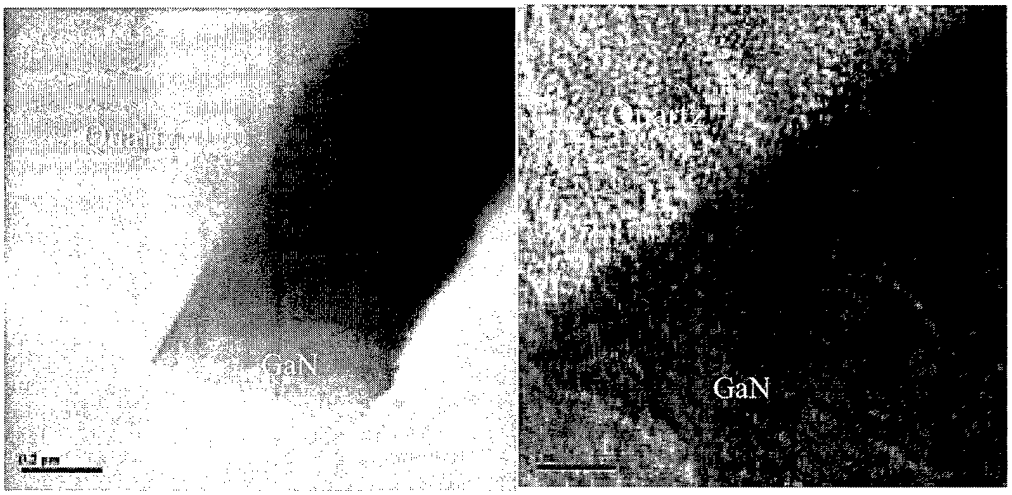

Figure 32. Cross sectional TEM image of a nanocrystalline GaN film on a quartz substrate

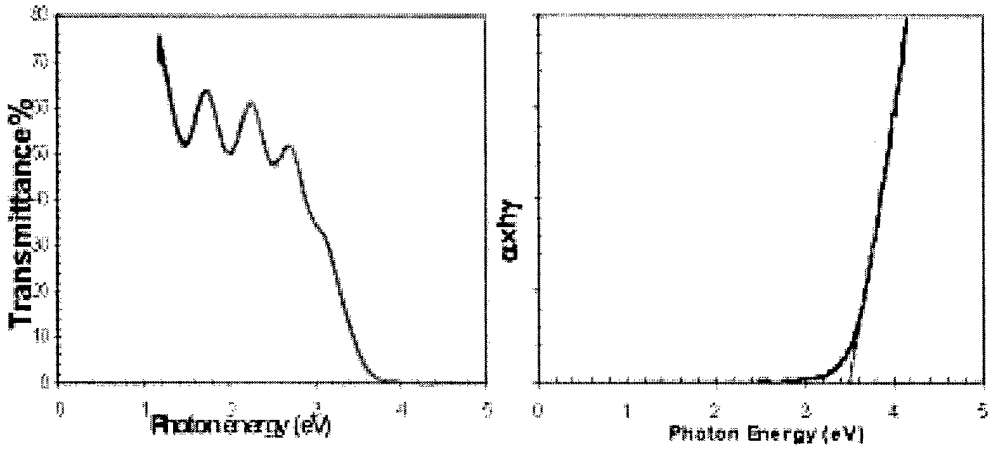

Figure 34. UV-Vis spectroscopy of nanocrystalline GaN film on a quartz substrate. The band gap was determined to be 3.4 eV.

6.0 Bulk synthesis of GaN and related nanostructures

6.1. GaN One-dimensional Nanostructures

Some interesting one-dimensional GaN nanostructures were discovered during the nitridation experiments. Long straight nano-wires 40nm in diameter with aspect ratios greater than 20 were observed on polycrystalline GaN films (Fig. 35(a)). The HRTEM micrograph of one nanowire is shown in Fig. 34(b) and indicates single crystal hexagonal GaN. The inserted SADP in Fig. 35(b) indicates the growth direction to be <10-10>. The deprivation of molten gallium films with N_2 plasma at high temperatures might curtail lateral growth and promote the growth of GaN nanowires.

Addition of a small amount of hydrogen during the nitridation of thin gallium films under normal conditions yields the growth of tapered and straight GaN whiskers occurred as seen in Fig. 35 (c) & (d). Some tapered whiskers have a triangular cross section as shown in Fig. 35(d). The growth direction of the nanowires was observed to be <001> from HRTEM analysis. Some experiments were also performed in a hot-filament reactor using ammonia. Nanowires with random branches as small as 10 nm were synthesized (Fig. 36). These results indicate that hydrogen plays a role in the formation of these unusual morphologies. The results also demonstrate that the characteristics of the resulting nanowires such as diameter and growth direction can be changed by varying the gas phase composition during the bulk synthesis of GaN nanowires from molten gallium.

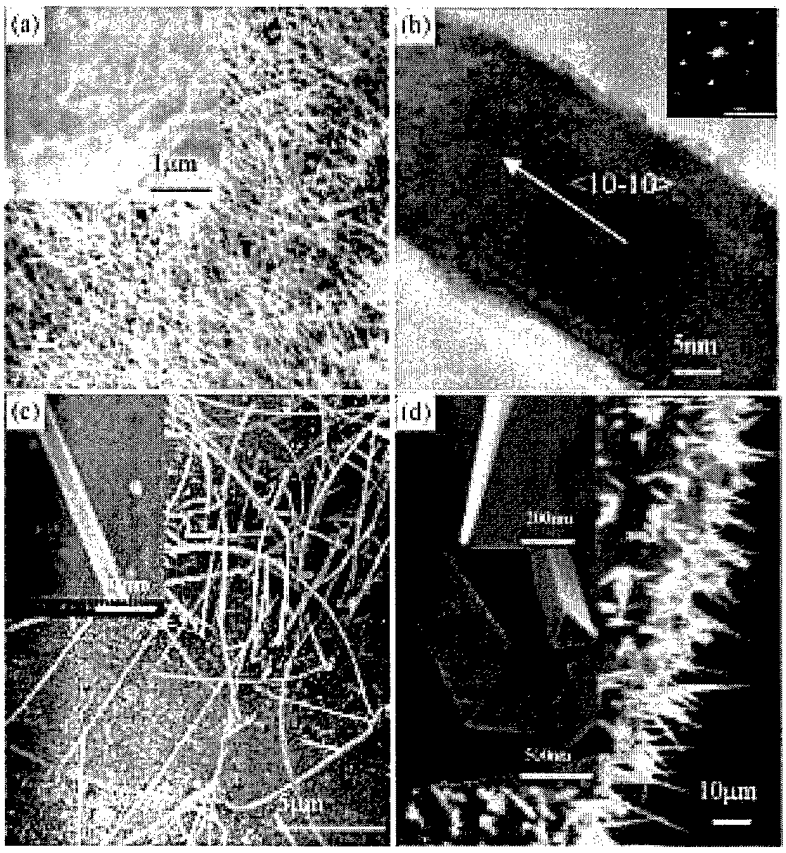

Figure 35. (a)&(b) GaN nanowires grown from polyscrystalline GaN (b) HRTEM of one nanowire shows single crystalline GaN and a growth direction of <10-10>; (c)&(d) GaN nanowires from addition of atomic hydrogen (d) Tapered GaN whiskers with a triangle cross section;

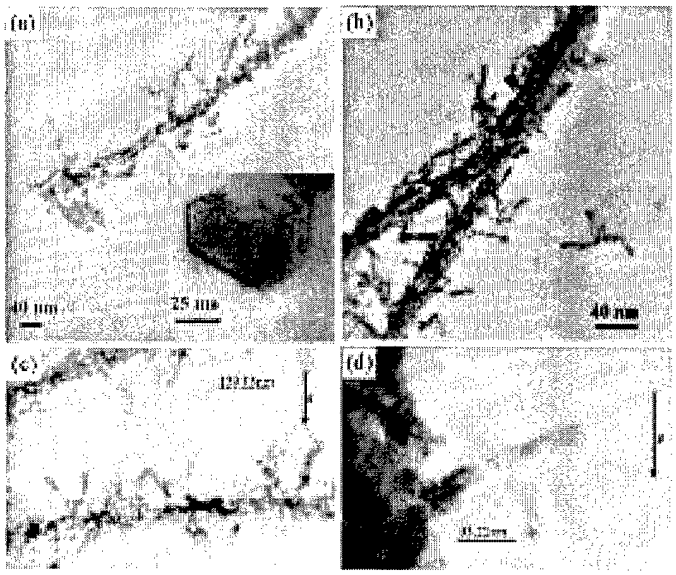

Figure 36. TEM images of branched GaN nanowires with NH_3 in a hot-filament reactor

Experiments performed to study the growth of GaN on previously synthesized GaN nanowires led to the formation of faceted crystals at each end of the nanowires as shown in Figure 37 (b). The evaporation of Ga onto existing GaN nanowires led to a necklace type morphology with Ga island decorations on the nanowires. The epitaxial growth of GaN on existing nanowires is even more fascinating since the growth seems to proceed mostly from either end indicating that the surface transport of adatoms is much faster. The entire nanowire acts like an antenna for the collection of vapor phase adatoms and supply to the growing epi-island on the nanowire. This mode of growth resulted in an interesting set of morphologies, i.e., spin-top and plate-shaped crystals continuously graded to long nanowires (> 100 microns). The most important outcome of these studies is that the surface transport of adatoms on sub-20 nm nanowires could be ballistic. Further studies are currently being performed to study this behavior and to synthesize hetero-junctioned nanowires using this method. The hetero-epitaxial growth of other semiconductor and metallic materials onto the existing sub-20 nm GaN nanowires should lead to hetero-nanostructures for easy integration using contacts.

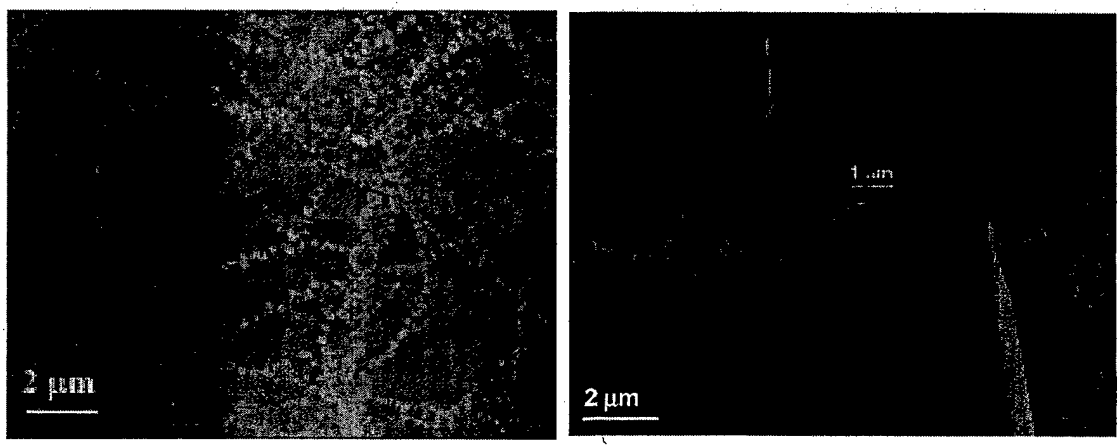

Figure 37. (a) Epitaxial growth of GaN crystals on GaN nanowires. (a) Formation of Ga islands during initial stages of growth due to high surface diffusion of Ga atoms. (b) Epitaxial growth of GaN crystals on GaN nanowires (Note that the diameter of the nanowires is as small as 20 nm).

6.2. InN Nanowire Synthesis

Indium nitride nanowires have been synthesized using the chemical vapor transport of indium, in the presence of ammonia, onto substrates maintained at a temperature of 600 °C. The experiments were performed in a hot-filament chemical vapor deposition (HFCVD) setup at 2 torr pressure. A schematic representation of the experimental setup is shown in Figure 38. Pure indium (Alfa Aesar, 99.99 % purity) was placed in a boron nitride crucible and heated to a temperature of about 700°C. The substrate was placed on top of the crucible, so that it partially covered the top of the crucible. 140 sccm of pure ammonia was used for the nanowire synthesis experiments. Indium vaporizing from the crucible is transported onto the substrates, and in the presence of ammonia results in InN nanowire formation on the substrate. Various substrates used for the synthesis of InN nanowires include quartz, R-plane oriented sapphire, polycrystalline AlN and highly ordered pyrolytic graphite (HOPG). SEM of the resulting InN nanowires is presented in Figure 39.

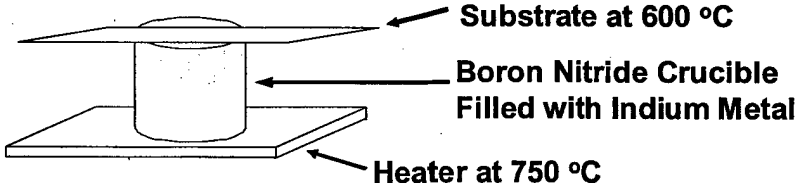

Figure 38. Schematic representation of the experimental setup used for the synthesis of InN nanowires.

Figures 39(c)&(d) demonstrate that the oriented growth of InN can be achieved using the bulk synthesis method, without the need of any catalyst clusters or templates. Scanning tunneling spectroscopy of the InN nanowires synthesized on HOPG was performed under UHV conditions and the current (I) .vs. voltage (V) characteristics are

presented in Figure 40. From the IV curve, the bandgap of the synthesized nanowires was determined to be 0.8 eV.

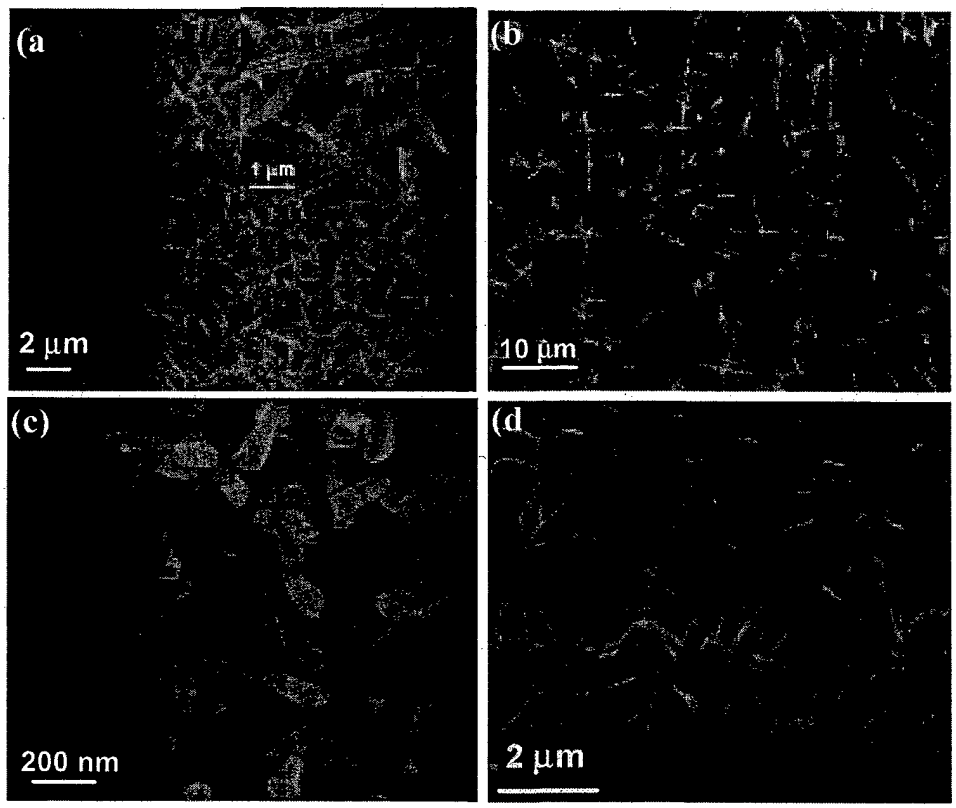

Figure 39. (a) Branched InN nanowires synthesized using the chemical vapor transport of In in the presence of NH_3. The diameter of the branches is approximately 50 nm. High magnification image of the branched nanowires is shown in the insert. (b) and (c) branched nanowires synthesized on polycrystalline AlN substrate. (c) InN nitride nanowires synthesized epitaxially on aluminum nitride substrate. (d) Oriented growth of InN nanowires on a polished R-plane oriented sapphire substrate.

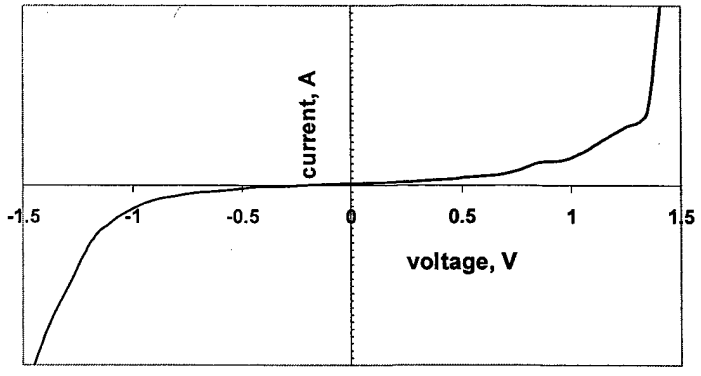

Figure 40. STS IV curve of the synthesized InN nanowires, showing the bandgap of the nanowires to be approximately 0.8 eV.

7.0 Miscellaneous Results

7.1. Optical measurements

The Raman spectrum was taken using a 632.8nm HeNe laser at room temperature with a Renishaw InVia Raman microscope. The spectrum in normal back-scattered configuration under which only E2 and A1 (LO) modes are allowed for hexagonal GaN [30] is shown as curve 'a' in Fig. 41(a). The spectrum shows the characteristic peaks of E_2^1 at 143cm-1, E_2^2 at 567 cm-1.and A1(LO) at 739 cm-1. Curve b in Fig. 41(a) is the Raman spectrum measured with the laser focus on the cross section of the GaN film where the incident beam is perpendicular to the c-axis. The $A_1(TO)$ mode at 531cm-1, $E_1(TO)$ mode at 559cm-1 and $E_1(LO)$ mode at 743cm-1 that are absent in the back scattering configuration show up. Fig. 41(b) shows the photoluminescence spectrum of the GaN flakes with a 325nm He-Cd UV laser. There is a strong near band edge emission centered at 3.39eV with a FWHM of 0.13eV. The band gap matches very well with the literature for wurtzite GaN [36].

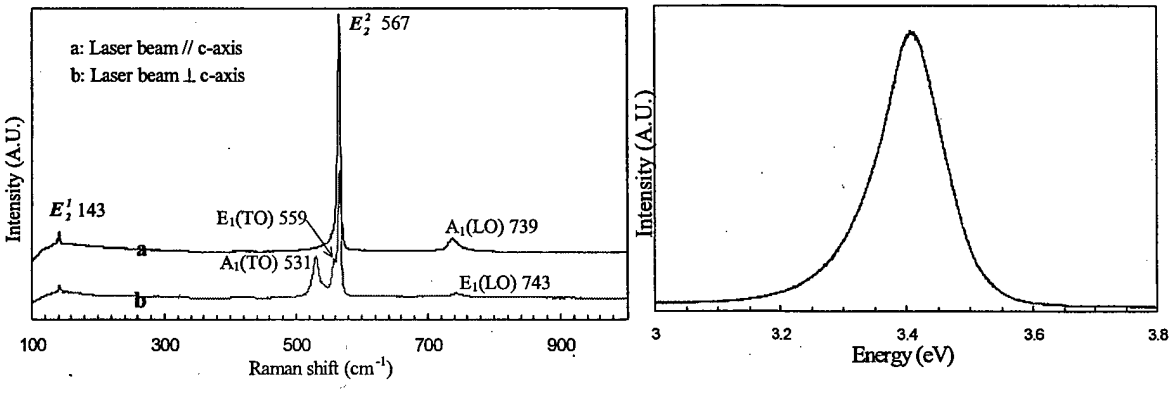

Figure 41. Raman spectrum obtained using back-scattered configuration for one of the resulting GaN films.

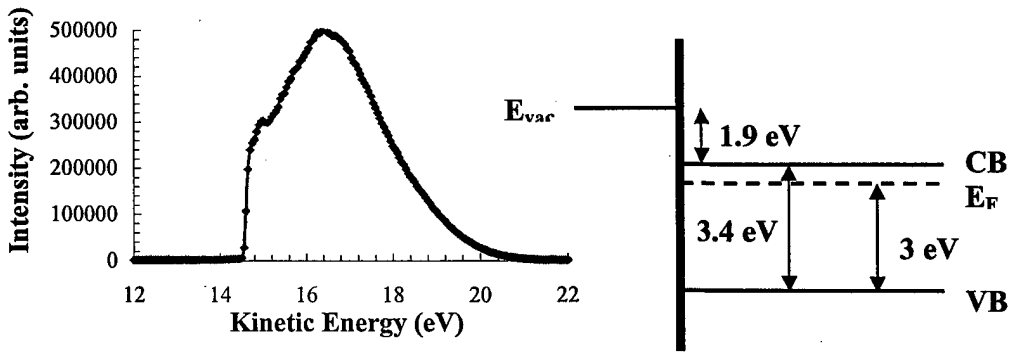

Figure 42. (a) Overall UPS spectra obtained from Gallium Nitride flake. (b) the band structure of the GaN flake indicates n-type characteristics, which may be due to oxygen contamination.

Ultra-violet photoelectron spectroscopy was performed on GaN to mainly determine the valence band structure of the sample. A flake of GaN was mounted on a silver foil, and the sample was exposed to ultraviolet light from the He lamp (at He I radiation = 21.2eV). Fig. 42 shows the UPS spectrum of the sample and the corresponding band structure. The sample was found to be n-type, possibly due to oxygen contamination. Scanning tunneling microscopy and spectroscopy were performed on the GaN flake to determine defect states, band gap, and surface morphology (Fig. 43). The bandgap was found to be around 3.3-3.4eV.

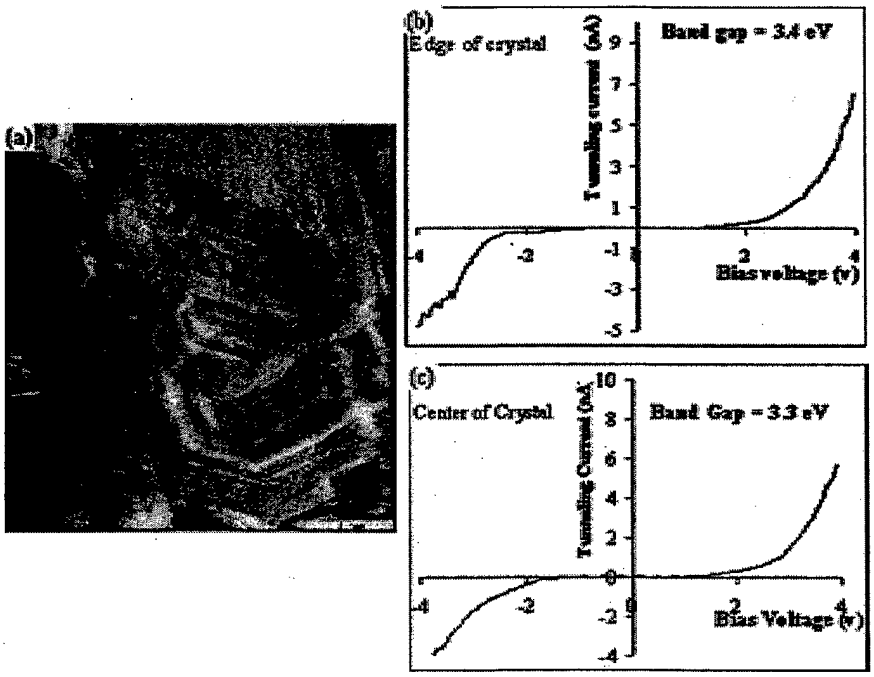

Figure 43. (a) Morphology of GaN crystals grown on quartz substrate; (b) the I-V curve obtained from the grain boundary shows a band gap of 3.4 eV; (c) the I-V curve obtained from the center of the crystal shows a band gap of 3.3 eV.

7.2. Marangoni convection phenomena with temperature gradient

A set of experiments was performed using gallium film covered substrates on a flat alumina-coated filament heater as shown in Fig. 44. Both Pyrolytic boron nitride substrates and quartz substrates were used for this experiment employing similar experimental conditions as before.

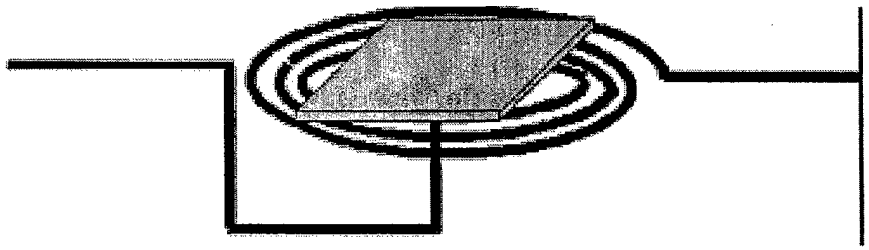

Figure 44. Flat alumina-coated filament heater assembly

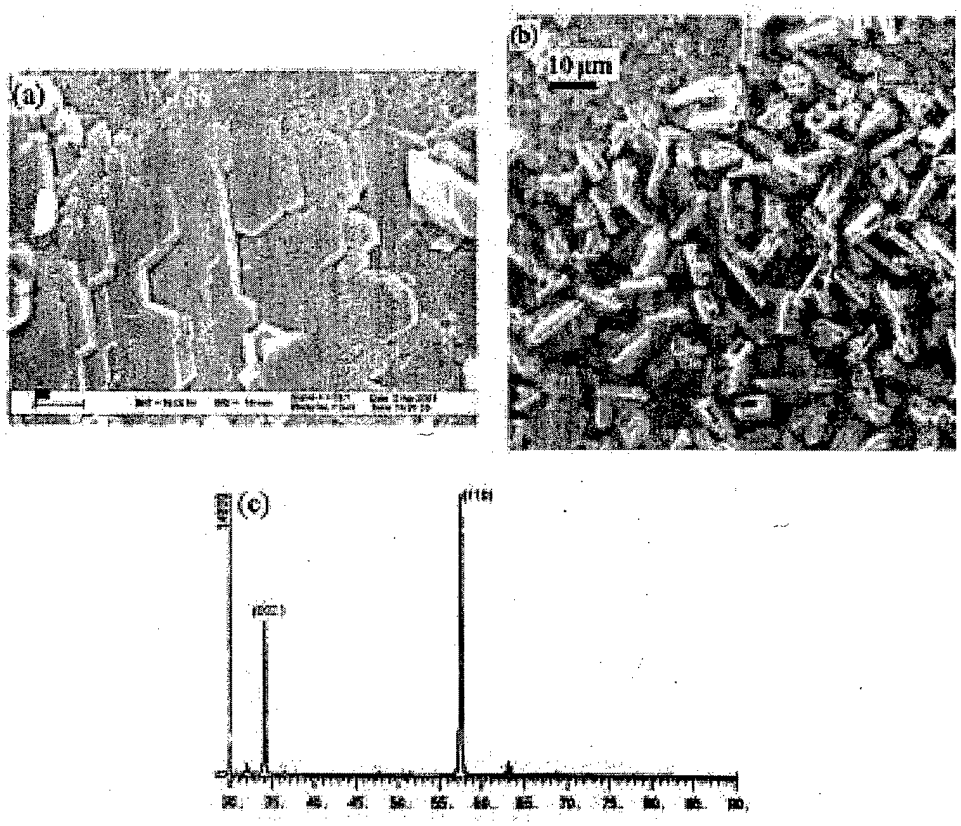

Figure 45. Both horizontal and vertically aligned hexagonal GaN platelets crystals on the substrates (a) large horizontal platelets; (b) vertically oriented platelets on quartz substrate. (c) XRD shows two primary reflections from (0002) and (11-20).

SEM images in Fig. 45(a) and (b) show that there are regions of both horizontal and vertically aligned hexagonal GaN platelets crystals on the substrates. The XRD spectrum in Fig. 45(c) indicates that the two different orientations are (0002) and (11-20). We think they resulted from a micro-flow phenomenon termed as Marangoni convection that gives rise to lateral temperature gradients for this particular heater set-up. Preliminary analysis of the molten gallium film on a stationary heated substrate stage suggests that the surface of the gallium tends to be stable at high frequencies or small wavelengths, which might cause vertical orientation, for thicknesses less than 50 μm. A mathematical analysis was carried out to understand the flow of molten gallium that occurs during Marangoni Convection. The analysis and discussion were focused on the onset and linear stability of Marangoni convection that occur in thin gallium films heated from below. A detailed analysis is presented in reference [25]. A few of the results from the analysis are shown in Figs. 46-48.

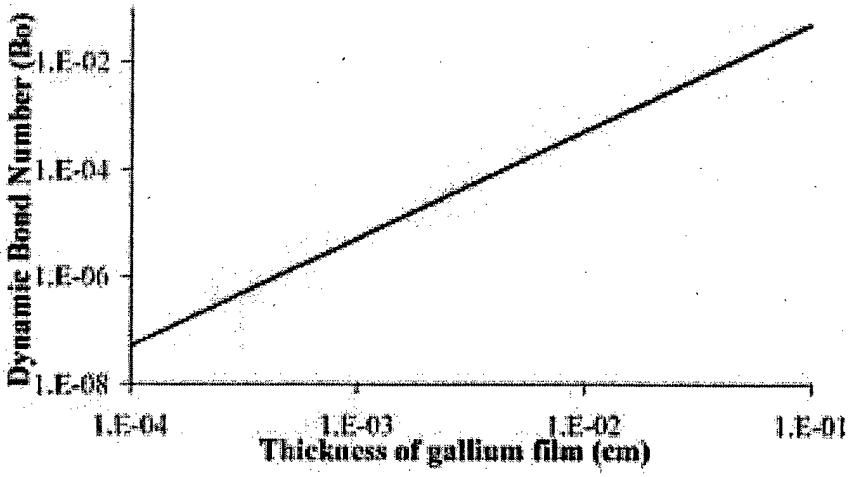

Figure 46. Dynamic Bond number as a function of gallium film thickness calculated at 1223K This indicates that capillary forces dominate over buoyant forces up to a thickness of ~1mm for gallium films.

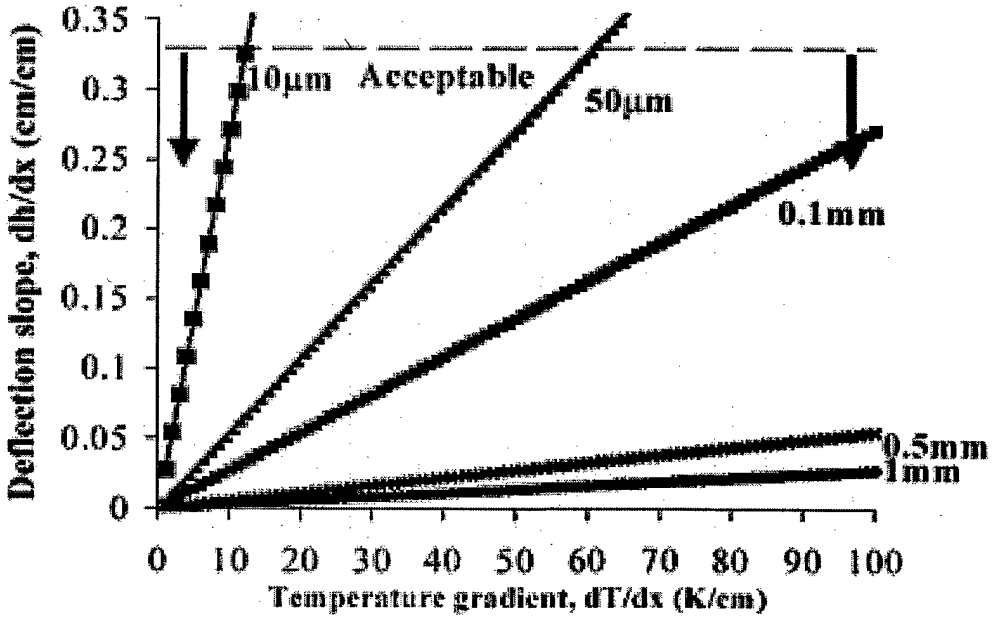

Figure 47. The surface deflection due to Marangoni Convection is determined as a function of lateral temperature gradient at different film thicknesses. The criterion for acceptability is assumed to be the same as the minimum aspect ratio for platelet shaped crystal.

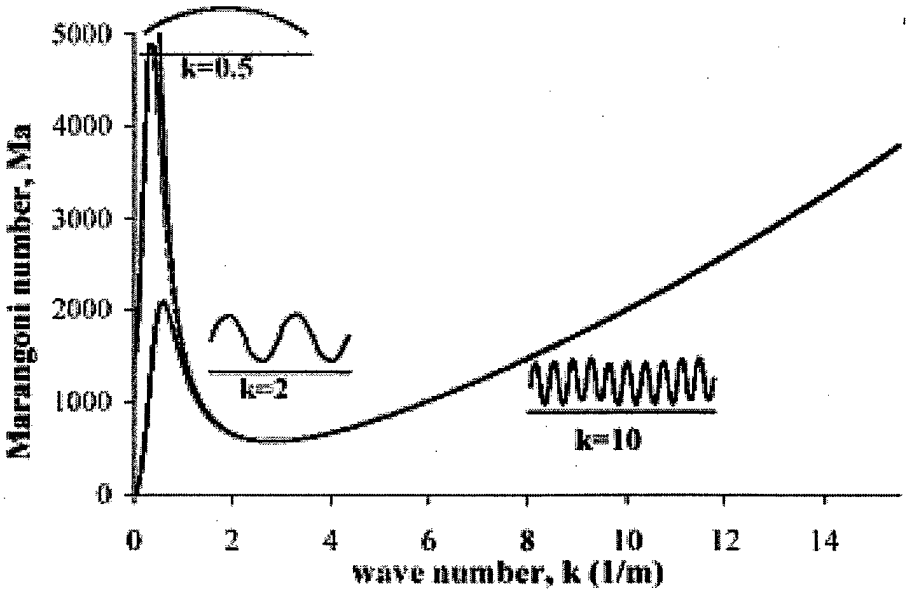

Figure 48. Critical Marangoni number is determined as a function of the wave number of the flow field in the neutral regime (linearly stable). The results illustrate that the Marangoni number will determine which type of flow field will be stable.

The experiments clearly demonstrate the concept of the self-oriented growth of GaN and suggest that one can accomplish the growth of single crystal quality GaN over larger areas without the use of hetero-epitaxy with underlying substrates. These results also strongly suggest that the flow patterns within molten gallium films during the nucleation and growth stages should be kept parallel to the substrate to achieve self-oriented growth over large areas (2 inch).

III Summary

The results from this project clearly demonstrate the concept for self-oriented GaN growth and suggest that one can accomplish the growth of single crystal quality GaN over larger areas without the use of hetero-epitaxy with underlying substrates. These results also strongly suggest that the flow patterns within molten gallium films during the nucleation and growth stages should be kept parallel to the substrate to achieve self-oriented growth over large areas (2 inch).

- Experiments using pools of molten gallium formed C-plane oriented dome shaped GaN flakes. Experiments using amorphous substrates immersed in molten Ga formed self-oriented GaN flakes. Subsequent experimentation using nitridation of molten Ga covered substrates resulted in highly oriented GaN films directly on molten Ga.

- The nitridation experiments clearly indicated that the flow and the wetting behavior changes with dissolved nitrogen in the melt. The spreading also varies with the interaction of the gallium with the substrate. It was observed that gallium wets fused silica substrates better than polycrystalline AlN, and pBN. The flow of the nitrogenated melt (wetting) during the nucleation and growth of GaN crystals proved to be a necessary condition for the formation of highly oriented GaN film formation. Once a GaN crust forms on top of molten Ga (either oriented or polycrystalline), the underlying Ga tries to flow out.

- Our investigations on the nucleation kinetics suggested that the domain size of GaN crystals depends on the mass of the molten gallium initially present. These results clearly indicated that the nucleation of GaN from molten Ga is a bulk phenomenon and is not a surface phenomenon.

- Mechanistic studies suggest that self-orientation occurs during early stages of GaN film formation on molten gallium. Further thickening of GaN occurs with LPE, suggesting that in-situ delivery of molten gallium could provide a viable process to increase the thickness of the GaN flakes into several mm thick ingots.

- Detailed study on the orientation and quality of the synthesized GaN films revealed that the GaN crystals joined at boundaries yielding low-angle grain boundaries. The quality of the joining of individual crystals was also studied using extensive TEM characterization. The evidence suggests that no dislocation crops are present in the crystals as expected. Cross sectional TEM analysis indicated single crystal quality films with rotational twists varying from 2-10 degrees between the adjacent columns while showing no dislocation contrast within the film. The self-orientation of the crystals observed within the films was hypothesized to have occurred from attachment at the boundary during coalescence.

- Nitridation of very thin films of gallium (<1μm) formed c-plane textured, nanocrystalline GaN over a large area.

- By varying the process conditions such as temperature, plasma conditions and hydrogen concentration, a variety of morphologies ranging from hollow crystals to star shaped crystals of GaN were obtained.

- The use of hydrogen along with nitrogen in plasmas allowed for the multiple nucleation and growth of GaN nanowires from Ga melts. Also, the diameter of the wires was varied from sub 10 nm to microns in this approach. This type of nanowire synthesis is quite different from various reports in literature. Here, the nanowire diameter is controlled by the size of the nuclei rather than the droplets at the tip, and the growth is due to basal attachment rather than attachment at tip. No catalyst metals such as gold were used. Both C-plane and edge plane oriented GaN nanowires were synthesized without the aid of hetero-epitaxial substrate orientations and were due to changes in the experimental conditions. Thermal excitation of ammonia over gallium and indium were also conducted to synthesize nanowires of GaN and InN.

- The homo-epitaxy experiments onto GaN nanowires using evaporation of Ga in an ammonia environment allowed for formation of fascinating morphologies, i.e., micron scale crystals at one end of the nanowires or grown intermittently over long GaN nanowires (> 100 microns). These results suggest that the adatom migration over sub 20 nm sized nanowires seems to be ballistic.

IV Publications And Patents Resulting From This Support

Publications resulting from this support directly on GaN:

1. H. Li, H. Chandrasekaran, M. K Sunkara, "Growth of Oriented Gallium Nitride Films Directly on Molten Gallium", Accepted, MRS 2004 Proceedings of Symposium E, (2004).
2. H. Li, M. K Sunkara, A. Berezin, S. I. Borenstain, "Cathodoluminescence and Scintillation of GaN on Sapphire", to be submitted.
3. H. Li, H. Chandrasekaran, M. K. Sunkara, M. Stukowski, K. Rajan, "Self Oriented Growth of GaN Films on Molten Gallium", in "*State -of-the-Art Program on Compound Semiconductors XLI -and- Nitride and Wide Bandgap Semiconductors for Sensors, Photonics, and Electronics V*", Edited by H. Ng and A. G. Baca, The ECS Inc., NJ, (2004).
4. H. Li, H. Chandrasekaran, M. K. Sunkara, "*Growth of Oriented Gallium Nitride Films on Amorphous Substrates by Self Assembly*", MRS Symp. Proc., L3.11, 743, (2003)
5. S. Sharma, H. Li, H. Chandrasekaran, R. C. Mani, M. K. Sunkara, "Synthesis of Inorganic Nanowires and Nanotubes", in *Encylcopedia of Nanoscience and Nanotechnology*; Edited by H. Nalwa, American Scientific Publishers, Los Angeles, CA, (2003).
6. H. Li, M. K. Sunkara, "*Self Oriented Growth of Gallium Nitride Films on Amorphous Substrates*", Proceedings of the 4th Symposium on Non-Stoichiometric III-V Compounds, Ed., 105, Pacific Grove, CA, USA, (2002)
7. H. Chandrasekaran, M. K. Sunkara, "*Growth of Gallium Nitride Textured Films and Nanowires on Polycrystalline Substrates at sub-Atmospheric Pressures*", MRS Symp. Proc., I3.30, V693, (2002)

Publications resulting from this support but indirectly related to the proposed work on GaN, i.e., Ga as the molten solvent for synthesis of nanostructures.

1. S. Vaddiraju, H. Chandrasekaran and M.K. Sunkara, JACS, **25**(36) 10792-10793 (2003)
2. M.K. Sunkara, S. Sharma, H. Chandrasekaran, M. Talbott, K. Krogman, and G. Bhimarasetti, ***Invited Paper,*** J. Mater. Chem., 2004, **14**, 590-594 (2004).
3. U.M. Graham, S. Sharma, M.K. Sunkara, and B.H. Davis, Adv. Funct. Mater., **(featured on front cover)** 13 (7): 576-581 (2003).
4. G. Bhimarasetti, M.K. Sunkara, U.M. Graham, B.H. Davis, C. Suh, and K. Rajan, Advanced Materials ***(featured on front cover),*** 15 (19), 1629 (2003).
5. S. Sharma, M.K. Sunkara, and E.C. Dickey, "Direct Synthesis of Silicon Nanowires using Silane and Molten Gallium", Mat. Res. Soc. Symp. Proc., Vol 737, F6.2.1 (2002).
6. S. Sharma, M.K. Sunkara, U.M. Graham, and B.H. Davis, "Nucleation and Growth of Gallium Oxide Tubes, Nanopaintbrushes and Nanowires from Molten Gallium", Mat. Res. Soc. Symp. Proc. Vol. 755, DD9.4.1 (2002).

7. S. Sharma, M.K. Sunkara, G.D. Lian, and E.C. Dickey, "Bulk Synthesis of Silicon Nanowires from Molten Gallium using Silane Gas Phase Precursors", Proc. AIChE Fall Meeting, pp. 16 (2002).
8. S. Sharma and M.K. Sunkara, "Direct Synthesis of Gallium Oxide Tubes, Nanowires, and Nanopaintbrushes", J. Am. Chem. Soc. 124 (41), 12289 (2002).
9. M.K. Sunkara, S. Sharma, E.C. Dickey and R. Miranda, "Bulk Synthesis of Silicon Nanowires using Low Temperature Vapor-Liquid-Solid Growth of Silicon Nanowires", Appl. Phys. Lett., 79(10), 1546-1549 (2001).
10. M. K. Sunkara, S. Vaddiraju, and G. Bhimarasetti, in Role of Chemical Engineering in Processing of Minerals and Materials, Ed: J.N. Mohanty, S.K. Biswal, S.R. Reddy, P.V.N. Misra, Allied Publishers, New Delhi, India, 134-144 (Dec 2003).

U.S. Patents

1. U. Graham, S. Sharma, M.K. Sunkara and B.H. Davis, "Metal-Oxide Nanowebs: Synthesis and Applications", Provisional Patent filed,) 6/2003, US Patent Applied 06/2004.

2. G. Bhimarasetti, R.C. Mani and M.K. Sunkara, "Carbon Tubular Structures: Method for Making them and Using the Same", Provisional Patent Application Filed 6/2003. **A total three patent applications are currently being applied.**

3. S. Sharma and M.K. Sunkara, "Low Temperature Synthesis Route for Semiconductor Fibers", U.S. Provisional Patent No. 60/302,062 (06/2000); U.S. Utility Patent Application No. 09/896,834; U.S. Utility Patent Application No. 10/187,460. **First one allowed** and others are being considered.

4. H. Chandrasekaran, H. Li and M.K. Sunkara, "Bulk Synthesis of Metal and Metal Based Dielectric Nanowires", U.S. Provisional Patent Application No. 60/425,194.

5. S. Sharma and M.K. Sunkara, "Direct Synthesis of Oxide Nanostructures of Low-Melting Materials", U.S. Provisional Patent Application No. 60/411,116.

6. H. Chandrasekaran and M.K. Sunkara, "Growth of Textured Gallium Nitride Thin Films and Nanowires on Polycrystalline Substrates", U.S. Provisional Patent Application No. 60/376,492. **Allowed.**

V Collaborations

- Collaborated with Prof. Sitar at NCSU on XRD texture analysis of oriented flakes.
- Collaborated with Prof. K. Rajan at RPI for TEM analysis
- Collaborated with Prof. J. Chaudhuri at Wichita State for performing SWBXT analysis using the Standford facility.
- Collaborated with Dr. S. Borenstein at El-Mul Technologies (Israel) for performing time-resolved CL analysis.
- Collaborated with Prof. A.M. Rao at Clemons University on PL/Raman analysis
- Started to interact with Dr. David Look at Wright State on electronic properties measurements

VI References

1. H. Morkoc, S. N. Mohammad, *Science*, **267**, 51 (1995).
2. F. A. Ponce, D. P. Bour, *Nature*, **386**, 351 (1997).
3. M. A. Khan, M. S. Shur, *Mat. Sci. Eng. B-Solid*, **46**, 69 (1997).
4. S. A. Safvi, J. M. Redwing, M. A. Tischler, T. F. Kuech, *J. Electrochem. Soc.*, **144**, 1789 (1997).
5. L. T. Romano, B. S. Krusor, R. Singh, T. D. Moustakas, *J. Electron. Mater.*, **26**, 285 (1997).
6. R. J. Molnar, W. Gotz, L. T. Romano, N. M. Johnson, *J. Cryst. Growth*, **178**, 147 (1997).
7. S. Porowski, I. Grzegoty, *J. Cryst. Growth*, **178**, 174 (1997).
8. L. Liu, J. H. Edgar, *Mat. Sci. Eng. R*, **37**, 61 (2002).
9. H. Marchand, J. P. Ibbetson, P. T. Fini, P. Kozodoy, S. DenBaars, J. S. Speck, U. K. Mishra, *MRS Internet J. Nitride Semicond. Res.*, **3**, 3 (1998).
10. R. F. Davis, T. Gehrke, K. J. Linthicum, T. S. Zheleva, E. A. Preble, P. Rajagopal, M. Mehregany, *J. Cryst. Growth*, **225**, 134 (2001).
11. A. R. A. Zauner, E. Aret, W. J. P. van Enckevort, J. L. Weyher, S. Porowski, J. J. Schermer, *J. Cryst. Growth*, **240**, 14 (2002).
12. S. Porowski, *MRS Internet J. Nitride Semicond. Res.*, **4S1**, G1.3 (1999).
13. C. M. Balkas, Z. Sitar, T. Zheleva, L. Bergman, R. Nemanich, R. F. Davis, *J. Cryst. Growth*, **208**, 100 (2000).
14. D. R. Ketchum, J. W. Kolis, *J. Cryst. Growth*, **222**, 431 (2001).
15. H. Yamane, M. Shimada, S. J. Clarke, F. J. DiSalvo, *Chem. Mater.*, **9**, 413 (1997).
16. A. Argoitia, C. C. Hayman, J. C. Angus, L. Wang, J. S. Dyck, K. Kash, *Appl. Phys. Lett.*, **70**, 179 (1997).
17. R. Madar, G. Jacob, J. Hallais, R. Fruchart, *J. Cryst. Growth*, **31**, 197 (1975).
18. D. Elwell, R.S. Feigelson, M.M. Simkins, W.A. Tiller, *J. Cryst. Growth*, **66**, 45 (1984).
19. S. Porowski and I. Grzegory, J. Crystal Growth 178 (1997) 174,
20. J. Prywer, S. Krukowski, MRS Internet J. Nitride Semicond. Res. 3 (1998) 47
21. C. M. Balka, Z. Sitar, L. Bergman, I. K. Shmagin, J. F. Muth, R. Kolbas, R. J. Nemanich, R. F. Davis, J. Crystal Growth 208 (2000) 100.,
22. M. Callahan, M. Harris, M. Suscavage, D. Bliss, J. Bailey, MRS Internet J. Nitride Semicond. Res. 4 (1999) 10.
23. H. Shin, D. B. Thomson, R. Schlesser, R. F. Davis, Z. Sitar, J. Crystal Growth 241 (2002) 404.
24. W. R. Wilcox, J. Crystal Growth 65 (1983) 133.
25. Hari Chandrasekaran, M.S Thesis, University of Louisville, March 2002
26. R.A. Logan, C.D. Thurmond, J. Electrochem. Soc. 119 (1972) 1727.
27. K. Hiramatsu, K.a Nishiyama, M. Onishi, H. Mizutani, M Narukawa, A. Motogaito, H. Miyake, Y. Iyechika, T. Maeda, J. Crystal Growth 221 (2000) 316.
28. P. Hartman, P. Bennema, J. Crystal Growth 49 (1980) 145.
29. H. Shin, E. Arkun, D.B. Thomson, P. Miraglia, E. Preble, R. Schlesser, S. Wolter, Z. Sitar, R.F. Davis, J. Crystal Growth 236 (2002) 529.

30. A. Tabata, R. Enderlein, J. R. Leite, S. W. da Silva, J. C. Galzerani, D. Schikora, M. Kloidt, K. Lischka, *J. Appl. Phys.*, **79**, 4137 (1996).
31. F. Demangeot, J. Frandon, M. A. Renucci, C. Meny, O. Briot, R. L. Aulombard, *J. Appl. Phys.* 82, 1305 (1997)
32. Y. Yao, A. Tholen, *Nanotechnology*, **13**, 169 (2002).
33. A. Gemperle, J. Gemperlová, *Ultramicroscopy*, **60**, 207 (1995).
34. J. M. Zuo, J. C. Mabon, *WebEMAPS software*, University of Illinois at Urbana - Champaign; URL: http://emaps.mrl.uiuc.edu/
35. J. I. Pankove, Prentice-Hall, Inc., Englewood, NJ (1971)
36. M. E. Levinshtein, S. L. Rumyantsev, M. S. Shur, ed., Properties of Advanced Semiconductor Materials: GaN, AlN, InN, BN, SiC, SiGe, John Wiley & Sons, (2001).